Mechanical Systems and Signal Processing 212 (2024) 111269

Contents lists available at ScienceDirect

Mechanical Systems and Signal Processing

journal homepage: www.elsevier.com/locate/ymssp

Rotation of mode shapes in structural dynamics due to mass and stiffness perturbations

M. Aenlle, N. García-Fernández *, F. Pelayo

Department of Construction and Manufacturing Engineering, University of Oviedo, Gijón, Spain

ARTICLE INFO

Keywords:
Structural dynamic modification
Polar decomposition
QR decomposition
Rotation of mode shapes
Scaling
Shear

ABSTRACT

According to the structural dynamic modification theory, the perturbed mode shapes can be expressed as a linear combination of the unperturbed mode shapes through a transformation matrix $\boldsymbol{T}$. This matrix is proposed in this paper as a powerful technique to determine whether the discrepancies between two models can be attributed to differences in stiffness, in mass, or both. It is demonstrated that matrix $\boldsymbol{T}$ becomes a rotation matrix when there are no mass discrepancies. In the case of mass discrepancies, or a combination of mass and stiffness differences, matrix $\boldsymbol{T}$ can be decomposed into a product of a rotation matrix and a matrix containing information about the changes in scaling and in shear. The angle of rotation depends on the closeness of the modes, and large rotations can be obtained when the system presents closely spaced or repeated modes. The polar and the QR decompositions are used in this paper to factorize matrix $\boldsymbol{T}$ as a product of two matrices, one of them being a rotation matrix. A new version of the modal assurance criterion (MAC), denoted in this paper as rotated MAC or ROTMAC, is proposed to detect mass discrepancies between two models. The equations and the conclusions derived in this paper have been validated through numerical simulations on a 2-degrees-of-freedom system and by correlating a numerical model and an experimental model of a square laminated glass plate.

1. Introduction

In several applications within the field of structural dynamics, it is a common practice to consider an experimental model as a perturbation of another model, referred to as the unperturbed model. For instance, in model correlation and model updating methods [1,2], the experimental model is typically regarded as a perturbation of a numerical model. Similarly, in the context of damage detection [3], the experimental damaged model is considered a perturbation of the corresponding experimental undamaged model.

In the field of algebra, an eigenvalue perturbation problem is that of finding the eigenvectors and eigenvalues of a system A (perturbed model), which is obtained as a perturbation of a system B (unperturbed model) with known eigenvectors and eigenvalues [4,5]. The study of the sensitivity of eigenvalue problems is denoted as perturbation theory of matrix pencils [4] and allows to know the sensitivity of the eigenvectors and eigenvalues of the unperturbed system (System B) to changes of mass and/or stiffness.

Structural dynamic modification (SDM) is a technique to study the effects of structural modifications (material, geometry, etc.) on the dynamic behavior of a structural system [6–8]. Two different problems are usually considered for SDM: the direct problem and the inverse problem. The direct problem consists in determining the effect of a known perturbation [6]. On the other hand, the inverse problem tries to identify the most appropriate changes required to obtain the desired dynamic behavior [6]. Most of the research to

* Corresponding author.
E-mail address: garciafnatalia@uniovi.es (N. García-Fernández).

https://doi.org/10.1016/j.ymssp.2024.111269
Received 24 October 2023; Received in revised form 15 February 2024; Accepted 17 February 2024
Available online 26 February 2024

date has been focused on the inverse structural modification problem [9–12], whereas only a few papers can be tracked for the direct structural modification problem [7,13–16]. Moreover, very few studies have been devoted to distributed modifications [17–20]. P. Avitable [21] reviewed structural dynamic modification techniques and discussed key factors influencing the success of the modification process such as: truncation of modes, rotational DOF's, mode shape scaling, drive point measurements, rigid body modes, complex vs. proportional modes, etc. The eigenvalue problem derived from the SDM provides the natural frequencies of the perturbed system, and a transformation matrix (denoted in this paper as matrix $\boldsymbol{T}$) which relates the modal matrices of both systems so that the eigenvectors of model A can be expressed as a linear combination of the eigenvectors of the model B through this matrix $\boldsymbol{T}$ [6–8].

In experimental modal analysis, the mode shapes are only known at the measured or active DOF's, which can be expanded to the unmeasured DOF's using a numerical model and a transformation matrix relating the modal matrices of both systems [1,22]. In [23], the experimental mode shapes were expanded using a finite element model, allowing for a more accurate estimation of the length and the cross-length of the mode shapes. This transformation matrix can also be used to smooth the experimental mode shapes [1]. The optimal number of mode shapes to be considered in the estimation of matrix $\boldsymbol{T}$ was studied in [22]. Bernal [24] derived an analytical expression to estimate the modal masses of a dynamic system using the mass change method, where the diagonal terms of a transformation matrix $\boldsymbol{T}$, relating the modal matrices of both the perturbed and unperturbed systems, are needed.

Brincker and Aenlle [25]. demonstrated that when a system B with closely spaced eigenvalues is perturbed, the associated mode shapes mainly rotate in their initial subspace, i.e., matrix $\boldsymbol{T}$ is mainly a rotation matrix, and the maximum angle corresponds to the case of repeated modes. Moreover, from the sensitivity equations based upon a Taylor expansion [26,27], it is inferred that a perturbation induce changes in the scaling and in the relative angle between the mode shapes. Thus, the matrix $\boldsymbol{T}$ contains the effects of rotation, shear (relative angle between mode shapes) and changes in scaling, and for model correlation and model updating purposes, it would be very interesting to separate these effects. In linear algebra, a matrix factorization is a decomposition into a product of matrices [28,29]. There are various techniques available for the matrix factorization and in this paper the polar and QR decompositions will be used to separate the effects of the rotation (rotation matrix), and the effects of shear and scaling in another matrix. The polar decomposition separates a matrix into a unitary matrix and a Hermitian positive semi-definite matrix [30–32]. On the other hand, the QR decomposition factorizes a matrix into a unitary matrix and an upper triangular matrix [33–35].

Model correlation techniques are methods used to compare two different models, and they can be classified into various categories. The criteria based on eigenvalues compare a set of natural frequencies of two models, and the most commonly used method is the normalized relative frequency difference (NRFD) [36]. On the other hand, the criteria based on eigenvectors compare a set of mode shapes, and the Modal Assurance Criterion (MAC) [36,37] is also the most widely used technique. However, if the mode shapes rotate in a subspace, a good correlation can exist in terms of mass and stiffness between two models with closely spaced modes, but low values of modal assurance criterion (MAC) can result due to the rotation of the mode shapes.

Although matrix $\boldsymbol{T}$ relates the mode shapes of two models, it has not been considered in the literature as a correlation technique. In this paper, the transformation matrix $\boldsymbol{T}$ is factorized into a product of two matrices, one of them being a rotation matrix. It is demonstrated that if there are no discrepancies in terms of mass between the models A and B, matrix $\boldsymbol{T}$ becomes a pure rotation matrix. In the case of a mass change perturbation, matrix $\boldsymbol{T}$ can be decomposed into a rotation matrix and a matrix containing the effect of shear and scaling. Thus, the transformation matrix $\boldsymbol{T}$ can be used to determine whether the discrepancies between two models B and A can be attributed to differences in stiffness, mass or both. This information holds significant utility in the fields of model correlation, model updating and damage detection. Moreover, a new version of the modal assurance criterion, denoted in this paper as rotated MAC or ROTMAC, is also proposed. It is worth noting that the analysis conducted in this paper is limited to the classical eigenvalue problem related to the undamped case of a linear dynamic system.

The paper is organized as follows. Section 2 presents the basic theory of structural dynamic modification and the corresponding eigenvalue problem expressed in terms of eigenvalues and eigenvectors of the unperturbed structure. In section 3, the polar and the QR decompositions of matrix $\boldsymbol{T}$ are briefly outlined and particularized to stiffness changes, mass changes, and simultaneous stiffness and mass changes. The applications of matrix $\boldsymbol{T}$ factorization is detailed in section 4. Section 5 applies the equations proposed in this paper to determine the rotation of a two degrees of freedom (DOF) system, which is perturbed with stiffness change $(\Delta\boldsymbol{K})$, mass change $(\Delta\boldsymbol{M})$, and simultaneous mass and stiffness changes. In section 6, the correlation between a numerical model and an experimental model of a square laminated glass plate is examined using matrix $\boldsymbol{T}$. The conclusions of the paper are presented in section 7. Supplemental mathematical details can be found in the appendices.

2. Structural dynamic modification

In the case of no damping, the equation of motion of a structure subjected to a force $\boldsymbol{p}$ is given by Eq. (1) [38–40]:

$$\boldsymbol{M_B}\,\ddot{\boldsymbol{u}} + \boldsymbol{K_B}\,\boldsymbol{u} = \boldsymbol{p} \tag{1}$$

where $\boldsymbol{K_B}$ and $\boldsymbol{M_B}$ are the stiffness and the mass matrices, respectively. Hereafter, bold capital letters will be used for matrices and bold lowercase letters for vectors.

The homogeneous differential equation derived from Eq. (1) provides the eigenvalue equation shown in Eq. (2) [38–40]:

$$\left(\boldsymbol{K_B} - \omega_{bi}^2\boldsymbol{M_B}\right)\boldsymbol{b}_i = 0 \tag{2}$$

where ω_{bi}^2 and $\boldsymbol{b}_i$ are the i-th eigenvalue and eigenvector, respectively. This eigenvalue problem is known in numerical mathematics as

generalized eigenvalue problem.

If a dynamic modification given by the mass change $\Delta \boldsymbol{M}$ and stiffness change $\Delta \boldsymbol{K}$ matrices is applied to system B, according to the structural dynamic modification theory, the mass matrix of the modified (or perturbed) system $\boldsymbol{M_A}$ can be expressed as:

$$\boldsymbol{M_A} = \boldsymbol{M_B} + \Delta \boldsymbol{M} \tag{3}$$

and the stiffness matrix as:

$$\boldsymbol{K_A} = \boldsymbol{K_B} + \Delta \boldsymbol{K} \tag{4}$$

The new equation of motion of the perturbed system, denoted as system A, becomes [6,7]:

$$(\boldsymbol{M_B} + \Delta \mathbf{M})\ddot{\boldsymbol{u}} + (\boldsymbol{K_B} + \Delta \mathbf{K})\boldsymbol{u} = \boldsymbol{p} \tag{5}$$

The homogeneous differential equation derived from Eq. (5) provides the following eigenvalue equation for the i-th mode [6,7]:

$$(\boldsymbol{M_B} + \Delta \boldsymbol{M})\boldsymbol{a_i}\ \omega_{ai}^2 = (\boldsymbol{K_B} + \Delta \boldsymbol{K})\boldsymbol{a_i} \tag{6}$$

where ω_{ai} and $\boldsymbol{a_i}$ are the natural frequency and the eigenvector, respectively, of the i-th mode.

According to SDM [6,7], the modal shape matrix $\boldsymbol{A}$ of the perturbed structure can be expressed as a linear combination of the modal shape matrix of system B as:

$$\boldsymbol{A} = \boldsymbol{B}\ \boldsymbol{T} \tag{7}$$

where $\boldsymbol{T}$ is a transformation matrix and $\boldsymbol{B}$ is the modal shape matrix of system B.

If Eq. (3) is pre-multiplied by $\boldsymbol{A^T}$ and post-multiplied by $\boldsymbol{A}$, it becomes:

$$\boldsymbol{A^T M_A A} = \boldsymbol{A^T M_B A} + \boldsymbol{A^T \Delta M A} \tag{8}$$

The inner product $\boldsymbol{A^T M_A A}$ is a diagonal matrix containing the modal masses of the system A, i.e., $\boldsymbol{m_A} = \boldsymbol{A^T M_A A}$, which becomes an identity matrix in the case of mass-normalized mode shapes ($\boldsymbol{m_A} = \boldsymbol{I}$). On the other hand, the inner product $\boldsymbol{A^T M_B A}$ can also be expressed as:

$$\boldsymbol{A^T M_B A} = \boldsymbol{T^T B^T M_B B T} = \boldsymbol{T^T T} \tag{9}$$

Substitution of Eq. (9) in Eq. (8) gives:

$$\boldsymbol{I} = \boldsymbol{T^T T} + \boldsymbol{A^T \Delta M A} \tag{10}$$

Furthermore, if Eq. (4) is pre-multiplied by $\boldsymbol{A^T}$ and post-multiplied by $\boldsymbol{A}$, it becomes:

$$\boldsymbol{A^T K_A A} = \boldsymbol{A^T K_B A} + \boldsymbol{A^T \Delta K A} \tag{11}$$

which, in the case of mass-normalized mode shapes, can also be expressed as:

$$\boldsymbol{\omega_A^2} = \boldsymbol{T^T \omega_B^2 T} + \boldsymbol{A^T \Delta K A} \tag{12}$$

where $\boldsymbol{\omega_A^2}$ and $\boldsymbol{\omega_B^2}$ are diagonal matrices containing the natural frequencies of systems A and B, respectively.

2.1. *Stiffness change* ($\Delta \boldsymbol{K}$)

If there are no discrepancies in terms of mass between models A and B, $\Delta \boldsymbol{M} = 0$ and Eq. (10) results in:

$$\boldsymbol{I} = \boldsymbol{T_K^T T_K} \tag{13}$$

where $\boldsymbol{T_K}$ is the matrix $\boldsymbol{T}$ when the system is only perturbed with a stiffness change. As $\boldsymbol{T_K}$ is a real square matrix, it is inferred from Eq. (13) that $\boldsymbol{T_K}$ must be a rotation matrix.

If a rotation is involved in Eq. (7), it must be expressed as:

$$\boldsymbol{A^T} = \boldsymbol{R_K B^T} \tag{14}$$

where $\boldsymbol{R_K}$ indicates rotation matrix. From Eq. (7) and Eq. (14) it is derived that:

$$\boldsymbol{T_K^T} = \boldsymbol{R_K} \tag{15}$$

The same conclusion is formulated from the mass matrices $\boldsymbol{M_A}$ and $\boldsymbol{M_B}$. Given that no discrepancies exist in terms of mass between both systems, the mass matrices of systems A and B must be equal, i.e:

$$\boldsymbol{M}_A = \boldsymbol{M}_B \tag{16}$$

If both matrices are expressed in terms of mode shapes, Eq. (16) becomes:

$$\left(\boldsymbol{A}\boldsymbol{A}^T\right)^{-1} = \left(\boldsymbol{B}\boldsymbol{B}^T\right)^{-1} \tag{17}$$

Substitution of Eq. (14) in Eq. (17) leads to:

$$\left(\boldsymbol{B}\boldsymbol{T}_K\boldsymbol{T}_K^T\boldsymbol{B}^T\right)^{-1} = \left(\boldsymbol{B}\boldsymbol{B}^T\right)^{-1} \tag{18}$$

From which is inferred that the inner product $\boldsymbol{T}_K\boldsymbol{T}_K^T$ must be an identity matrix and, consequently, $\boldsymbol{T}_K^T$ must be a rotation matrix.

After these considerations it can be stated that:

If there are not mass discrepancies between the systems B and A, the transformation matrix $\boldsymbol{T}_K$ is a rotation matrix. These means that the scaling and the relative angle between mode shapes are not modified.

The angle of rotation is small in systems with well-separated modes, and it affects to the full set of mode shapes. On the other hand, large rotations can occur in the case of closely or repeated modes, but the rotations occur mainly in the subspace defined by the closely or repeated modes [25].

2.2. Mass change ($\Delta\boldsymbol{M}$)

From Eq. (12), it is inferred that if there are no discrepancies in terms of stiffness between systems A and B, $\boldsymbol{A}^T\Delta\boldsymbol{K}\boldsymbol{A} = 0$ and Eq. (12) results in:

$$\boldsymbol{\omega}_A^2 = \boldsymbol{T}_M^T\boldsymbol{\omega}_B^2\boldsymbol{T}_M \tag{19}$$

where $\boldsymbol{\omega}_A^2$ is a diagonal matrix containing the natural frequencies (squared) of system A and $\boldsymbol{T}_M$ is the matrix $\boldsymbol{T}$ when the system is only perturbed with a mass change. From Eq. (19) it is inferred that:

If there are not stiffness discrepancies between the systems B and A, the inner product $\boldsymbol{T}_M^T\boldsymbol{\omega}_B^2\boldsymbol{T}_M$ must be a diagonal matrix and the natural frequencies of both systems are related by:

$$\omega_{ai}^2 = \boldsymbol{t}_{Mi}^T\boldsymbol{\omega}_B^2\boldsymbol{t}_{Mi} \tag{20}$$

where $\boldsymbol{t}_{Mi}$ is the i-th column vector of matrix $\boldsymbol{T}_M$.

Furthermore, from Eq. (10) it is inferred that the inner product $\boldsymbol{T}_M^T\boldsymbol{T}_M$ is given by:

$$\boldsymbol{T}_M^T\boldsymbol{T}_M = \boldsymbol{I} - \boldsymbol{A}^T\Delta\boldsymbol{M}\boldsymbol{A} \tag{21}$$

which demonstrates that $\boldsymbol{T}_M$ cannot be a pure rotation, but it approximates a rotation matrix for small mass changes.

Additionally, from the sensitivity equations based upon a Taylor expansion [26,27] it is inferred that a mass change also induces changes in the scaling of the mode shapes and in the relative angle between the mode shapes (shear).

From these considerations, the transformation matrix $\boldsymbol{T}_M^T$ can be expressed as a combination of rotation $\boldsymbol{R}_M$, shear $\boldsymbol{T}_{sh}$ and scaling $\boldsymbol{T}_{sc}$, i.e.:

$$\boldsymbol{T}_M^T = \boldsymbol{T}_{sc}\boldsymbol{T}_{sh}\boldsymbol{R}_M \tag{22}$$

And the inner product $\boldsymbol{T}_M^T\boldsymbol{T}_M$ is given by:

$$\boldsymbol{T}_M^T\boldsymbol{T}_M = \boldsymbol{T}_{sc}\boldsymbol{T}_{sh}\boldsymbol{T}_{sh}^T\boldsymbol{T}_{sc}^T \tag{23}$$

Which removes the effect of the rotation.

Using the notation $\boldsymbol{T}_{ch} = \boldsymbol{T}_{sc}\boldsymbol{T}_{sh}$, Eq. (23) results in:

$$\boldsymbol{T}_M^T\boldsymbol{T}_M = \boldsymbol{T}_{ch}\boldsymbol{T}_{ch}^T \tag{24}$$

This is also demonstrated in Appendix A, particularizing Eq. (19) for a system with two modes.

Moreover, using Eq. (7), the mass matrix $\boldsymbol{M}_A$ can be expressed as:

$$\boldsymbol{M}_A = \left(\boldsymbol{A}\boldsymbol{A}^T\right)^{-1} = \left(\boldsymbol{B}\boldsymbol{T}_M\boldsymbol{T}_M^T\boldsymbol{B}^T\right)^{-1} \tag{25}$$

2.3. Mass and stinffness change ($\Delta \boldsymbol{K} + \Delta \boldsymbol{M}$)

In the case of simultaneous stiffness and mass changes, it can be considered that the perturbation is carried out in the following two steps (see Fig. 1):

1. Perturbation of system B with a stiffness change $\Delta \boldsymbol{K}$, defined with matrix $\boldsymbol{T}_{\boldsymbol{K}}$(which is a rotation matrix). It results in the perturbed system denoted as A1.
2. Perturbation of system A1 with a mass change $\Delta \boldsymbol{M}$ and defined with matrix $\boldsymbol{T}_{1\boldsymbol{M}}$.

Matrix $\boldsymbol{T}_{1\boldsymbol{M}}^{\boldsymbol{T}}$ can, in turns, be decomposed into a rotation, shear and scaling as:

$$\boldsymbol{T}_{1M} = \boldsymbol{R}_{1M}^{T}\boldsymbol{T}_{1sh}^{T}\boldsymbol{T}_{1sc}^{T} = \boldsymbol{R}_{1M}^{T}\boldsymbol{T}_{1ch}^{T} \tag{26}$$

On the other hand, the matrix $\boldsymbol{T}$ relating systems B and A can be expressed as:

$$\boldsymbol{T} = \boldsymbol{T}_{k}\boldsymbol{T}_{1M} \tag{27}$$

Substitution of Eq. (26) in Eq. (27) leads to:

$$\boldsymbol{T} = \boldsymbol{R}_{k}^{T}\boldsymbol{R}_{1M}^{T}\boldsymbol{T}_{1sh}^{T}\boldsymbol{T}_{1sc}^{T} = \boldsymbol{R}_{k}^{T}\boldsymbol{R}_{1M}^{T}\boldsymbol{T}_{1ch}^{T} \tag{28}$$

Finally, the inner product $\boldsymbol{T}^{\boldsymbol{T}}\boldsymbol{T}$ results in:

$$\boldsymbol{T}^{T}\boldsymbol{T} = \boldsymbol{T}_{1ch}\boldsymbol{T}_{1ch}^{T} \tag{29}$$

Which nullifies the effect of the rotations corresponding to both stiffness and mass changes. Equations (13), (24) and (29) demonstrate that the inner product $\boldsymbol{T}^{\boldsymbol{T}}\boldsymbol{T}$ cancel the effects of the rotations of the mode shapes.

3. Polar and QR decompositions of matrix T

In undamped systems the components of the mode shapes are real and, consequently, matrix $\boldsymbol{T}$ is real. If matrix $\boldsymbol{T}^{\boldsymbol{T}}$ is a real square non-singular matrix size $n \times n$, the left polar decomposition [30–32,41] factorizes matrix $\boldsymbol{T}^{\boldsymbol{T}}$ as:

$$\boldsymbol{T}^{T} = \boldsymbol{W}\boldsymbol{R} \tag{30}$$

where matrix $\boldsymbol{W}$ is a positive semi-definite Hermitian and matrix $\boldsymbol{R}$ is an orthonormal matrix, i.e. $\boldsymbol{R}^{\boldsymbol{T}} = \boldsymbol{R}^{-1}$. Matrix $\boldsymbol{R}$ is a rotation matrix when $det(\boldsymbol{T}^{\boldsymbol{T}}) > 0$ and a reflection when $det(\boldsymbol{T}^{\boldsymbol{T}}) < 0$ [42]. $\boldsymbol{R}$ is unique if $\boldsymbol{T}^{\boldsymbol{T}}$ is invertible, and $\boldsymbol{W}$ is always unique and equal to:

$$\boldsymbol{W} = \sqrt{\boldsymbol{T}\boldsymbol{T}^{\boldsymbol{T}}} \tag{31}$$

Matrix $\boldsymbol{T}^{\boldsymbol{T}}$ can also be factorized with the right polar decomposition [30–32,41] as:

$$\boldsymbol{T}^{T} = \boldsymbol{R}\boldsymbol{Z} \tag{32}$$

where $\boldsymbol{Z}$ is a positive semi-definite Hermitian matrix.

The QR decomposition [33–35] can also be used to factorize Matrix $\boldsymbol{T}^{\boldsymbol{T}}$ as:

$$\boldsymbol{T}^{T} = \boldsymbol{R}\boldsymbol{Q} \tag{33}$$

If matrix $\boldsymbol{T}^{\boldsymbol{T}}$ is a real square non-singular matrix size $n \times n$, matrix $\boldsymbol{R}$ is an orthonormal matrix (it is unique) and $\boldsymbol{Q}$ is an upper triangular matrix (unique if $\boldsymbol{T}^{\boldsymbol{T}}$ is full rank).

The mathematical explanation of these factorizations is presented in Appendix B.

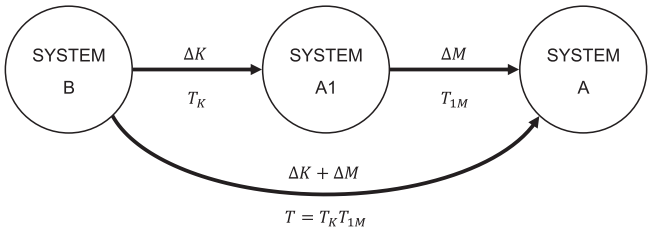

Fig. 1. Mass and stiffness perturbation of system B. System A1 is obtained perturbating system B with ΔK. System A is obtained perturbating system B with $\Delta K + \Delta M$. System A can also be obtained perturbating system A1 with.ΔM.

3.1. Decomposition of matrix $\boldsymbol{T}$ due to a stiffness change ($\Delta\boldsymbol{K}$)

If there are only discrepancies in stiffness, matrix $\boldsymbol{T}_k^T$ is a pure rotation, and the matrices $\boldsymbol{W}$ and $\boldsymbol{Z}$ obtained with the polar decomposition will be identity matrices in the case of mass-normalized mode shapes, or diagonal matrices in the case of unscaled mode shapes.

If matrix $\boldsymbol{T}_K$ is factorized with the QR decomposition (the decomposition of the matrix $\boldsymbol{T}^T$ into an orthogonal matrix and a triangular matrix), matrix $\boldsymbol{Q}$ is also an identity matrix in the case of mass-normalized mode shapes.

Therefore, the same rotation matrix is obtained with the polar and the QR decompositions, and moreover, $\boldsymbol{W} = \boldsymbol{Q}$. Thus, the polar decomposition or the QR decomposition are useful tools to determine if there are mass discrepancies between systems A and B. Identity matrices $\boldsymbol{W}$, $\boldsymbol{Z}$ and $\boldsymbol{Q}$ (in the case of mass-normalized mode shapes) are indicators of no discrepancies in terms of mass.

3.2. Decomposition of matrix $\boldsymbol{T}$ due to a mass change ($\Delta\boldsymbol{M}$)

If there are only mass discrepancies, the polar decomposition of matrix $\boldsymbol{T}_M$ gives:

$$\boldsymbol{R} = \boldsymbol{R}_M \tag{34}$$

and

$$\boldsymbol{W} = \boldsymbol{T}_{sc}\boldsymbol{T}_{sh} \tag{35}$$

The rotation matrix $\boldsymbol{R}$ obtained with the polar decomposition has the important property that it is the closest matrix with orthonormal columns to $\boldsymbol{T}_M$ in any unitarily invariant norm [43]. In a system with two modes and two DOF's this means that the angle γ between the vectors of matrix $\boldsymbol{T}$ and the vectors of matrix $\boldsymbol{R}$ (which are orthogonal) is minimum (Fig. 2). It the length of the mode shapes is similar,

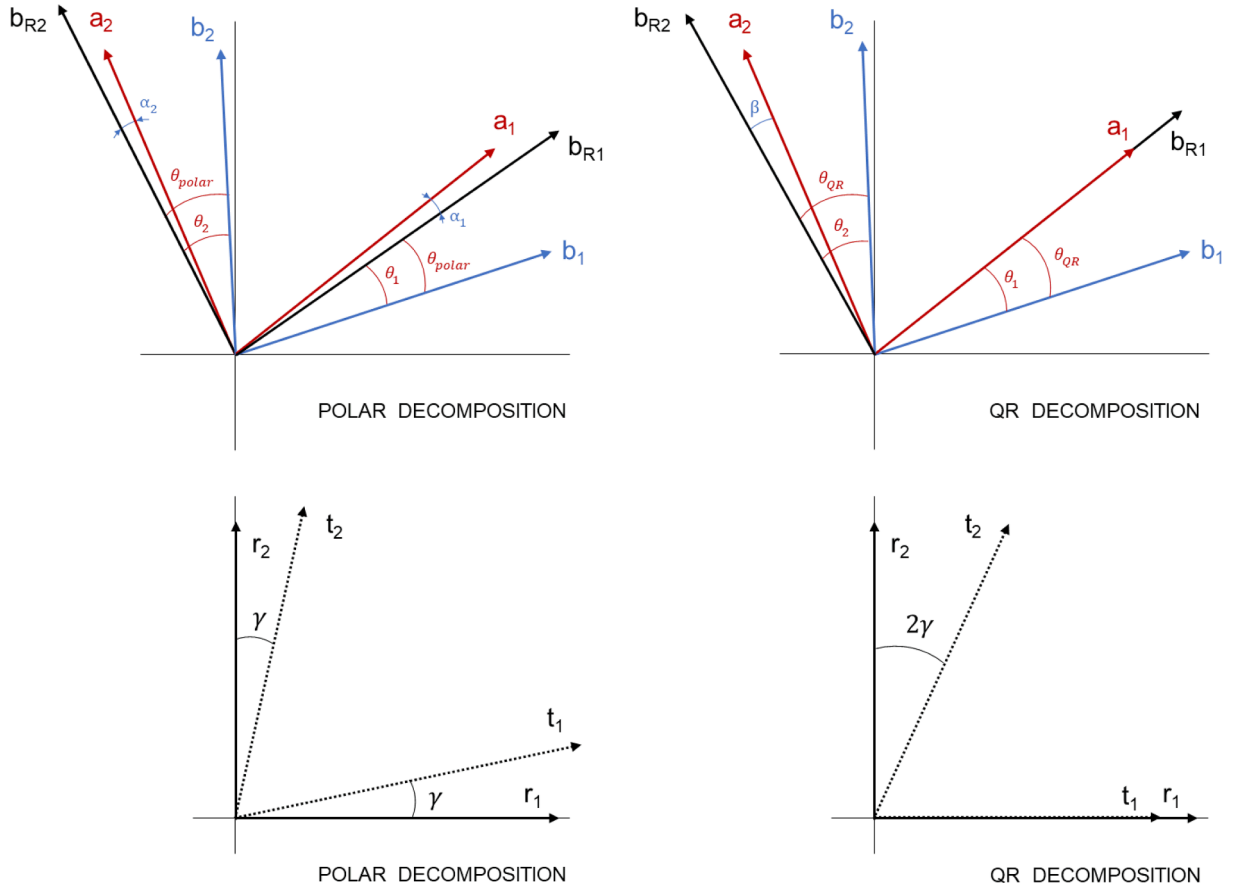

Fig. 2. Above) Rotation of mode shapes with polar and QR decomposition for a mass change. Below) Angles between the vectors of matrices $\boldsymbol{T}$ and $\boldsymbol{R}$ with the polar and QR decompositions. θ_{polar}: angle of rotation of mode shapes of system B when using polar decomposition. θ_{QR}: angle of rotation of mode shapes of system B when using QR decomposition. θ_1: angle between $\boldsymbol{b}_{R1}$ and $\boldsymbol{a}_1$. θ_2: angle between $\boldsymbol{b}_{R2}$ and $\boldsymbol{a}_2$. α_1: angle between $\boldsymbol{b}_{R1}$ and $\boldsymbol{a}_1$ (polar). α_2: angle between $\boldsymbol{b}_{R2}$ and $\boldsymbol{a}_2$ (polar). β: angle between $\boldsymbol{b}_{R2}$ and $\boldsymbol{a}_2$ (QR).

this also means that the angles α_1 and α_2 between the vectors of matrix $\boldsymbol{A}$ and the vectors of matrix $\boldsymbol{B_R}$, is similar.

If the QR decomposition is used, a slightly different rotation matrix is obtained, because matrix $\boldsymbol{Q}$ is triangular. In a system with two modes and two DOF's this means that one of the vectors of matrix $\boldsymbol{T}$ coincides with one of the vectors of matrix $\boldsymbol{R}$ (Fig. 2). This also means that one the mode shapes of system A coincides with the corresponding rotated mode shape (modes $\boldsymbol{b_{R1}}$ and $\boldsymbol{b_{R2}}$ in Fig. 2), whereas the angle between the other set of mode shapes is approximately $\beta \cong \alpha_1 + \alpha_2$.

The differences between the polar and the QR decompositions are shown in Appendix C with a 2 DOF example.

It must be noticed that using the polar decomposition, matrix $\boldsymbol{T_M^T}$ can be decomposed as:

$$\boldsymbol{T_M^T} = \boldsymbol{R_M Z} \tag{36}$$

And the mass matrix $\boldsymbol{M_A}$ can be expressed as:

$$\boldsymbol{M_A} = \left(\boldsymbol{B T_M T_M^T B^T}\right)^{-1} = \left(\boldsymbol{B Z^T R_M^T R_M Z B^T}\right)^{-1} = \left(\boldsymbol{B Z^T Z B^T}\right)^{-1} \tag{37}$$

Which confirms that a rotation of the mode shapes does not modify the mass matrix of a system.

3.3. Decomposition of matrix T due to a mass and stiffness change

If there are discrepancies in mass and stiffness, the polar decomposition of $\boldsymbol{T^T}$ gives:

$$\boldsymbol{R} = \boldsymbol{R_{1M} R_K} \tag{38}$$

i.e., the matrix $\boldsymbol{R}$ contains the effect of the rotation due to both mass and stiffness changes. Additionally, matrix $\boldsymbol{W}$ is given by:

$$\boldsymbol{W} = \boldsymbol{T_{1sc} T_{1sh}} \tag{39}$$

Again, the rotation matrices obtained with the polar decomposition and the QR decomposition are slightly different.

4. The concept of ROTMAC

Model correlation techniques are methods used to compare two different models, typically a numerical model with an experimental model. The Modal Assurance Criterion (MAC) [37] is by far the most widely used technique to compare mode shapes. If two vectors, $\boldsymbol{b_i}$ (model B) and $\boldsymbol{a_j}$ (model A), are compared, the MAC is given by Eq (40):

$$MAC\left(\boldsymbol{b}_i, \boldsymbol{a}_j\right) = \frac{\left|\boldsymbol{b}_i^T \boldsymbol{a}_j\right|^2}{\left(\boldsymbol{b}_i^T \boldsymbol{b}_i\right)\left(\boldsymbol{a}_j^T \boldsymbol{a}_j\right)} \tag{40}$$

where the superindex 'T' indicates transpose. MAC is always a real value and when dealing with complex vectors, the MAC is calculated with Eq (41).

$$MAC\left(\boldsymbol{b}_i, \boldsymbol{a}_j\right) = \frac{\left|\boldsymbol{b}_i^H \boldsymbol{a}_j\right|^2}{\left(\boldsymbol{b}_i^H \boldsymbol{b}_i\right)\left(\boldsymbol{a}_j^H \boldsymbol{a}_j\right)} \tag{41}$$

where the subindex 'H' indicates complex conjugate.

Closely spaced modes are highly sensitive to small mass and stiffness perturbations of the system, and they mainly rotate within their subspace [25]. Therefore, even if the compared models present good correlation in terms of mass and stiffness, this rotation can lead to low MAC values.

In this paper, it is proposed to calculate the MAC rotating the mode shapes of system B. This new definition, denoted in this paper as the rotated MAC or ROTMAC, is expressed as:

$$ROTMAC\left(\boldsymbol{b}_{Ri}, \boldsymbol{a}_j\right) = \frac{\left|\boldsymbol{b}_{Ri}^T \boldsymbol{a}_j\right|^2}{\left(\boldsymbol{b}_{Ri}^T \boldsymbol{b}_{Ri}\right)\left(\boldsymbol{a}_j^T \boldsymbol{a}_j\right)} \tag{42}$$

where the rotated mode shapes ($\boldsymbol{B_R}$) are obtained with the expression:

$$\boldsymbol{B_R} = \boldsymbol{B R^T} \tag{43}$$

where $\boldsymbol{R}$ is the rotation matrix obtained from the polar or QR decompositions.

The modal assurance criterion is calculated with vectors normalized to the unit length and, consequently, the ROTMAC only provides information of the effect of shear. Thus, the ROTMAC must be an identity matrix in the following cases:

- The system B is perturbed with a stiffness change. This occurs because the rotated mode shapes $\boldsymbol{B_R}$ coincide with mode shapes $\boldsymbol{A}$, indicating no shear effect.

- The system B is perturbed with a mass change, but the system has repeated or closely spaced modes. This is because the effect of shear is negligible for repeated or closely spaced modes (see Appendix A).

Symmetric structures usually present several sets of repeated (or closely spaced) modes and other sets of separated modes [44]. In these structures, the diagonal terms of the ROTMAC must be unity in the sets of repeated or closely spaced modes and less than unity in the components corresponding to the separated modes.

In order to discriminate if the discrepancies between two modes are due to stiffness or mass changes, the concept of ROTMAC can be used in combination with the inner product $\boldsymbol{T}^T\boldsymbol{T}$, where the diagonal terms provide information about changes in scaling. Alternatively, the effect of changes in scaling can also be obtained from the diagonal terms of matrices $\boldsymbol{W}, \boldsymbol{Z}$ and $\boldsymbol{Q}$.

The main findings of the paper derived in the previous sections for only mass discrepancies or only stiffness discrepancies are graphically summarized in Fig. 3.

5. Simulation cases

In this section, the modal parameters of a 2 DOF system are obtained solving the corresponding eigenvalue problem using the

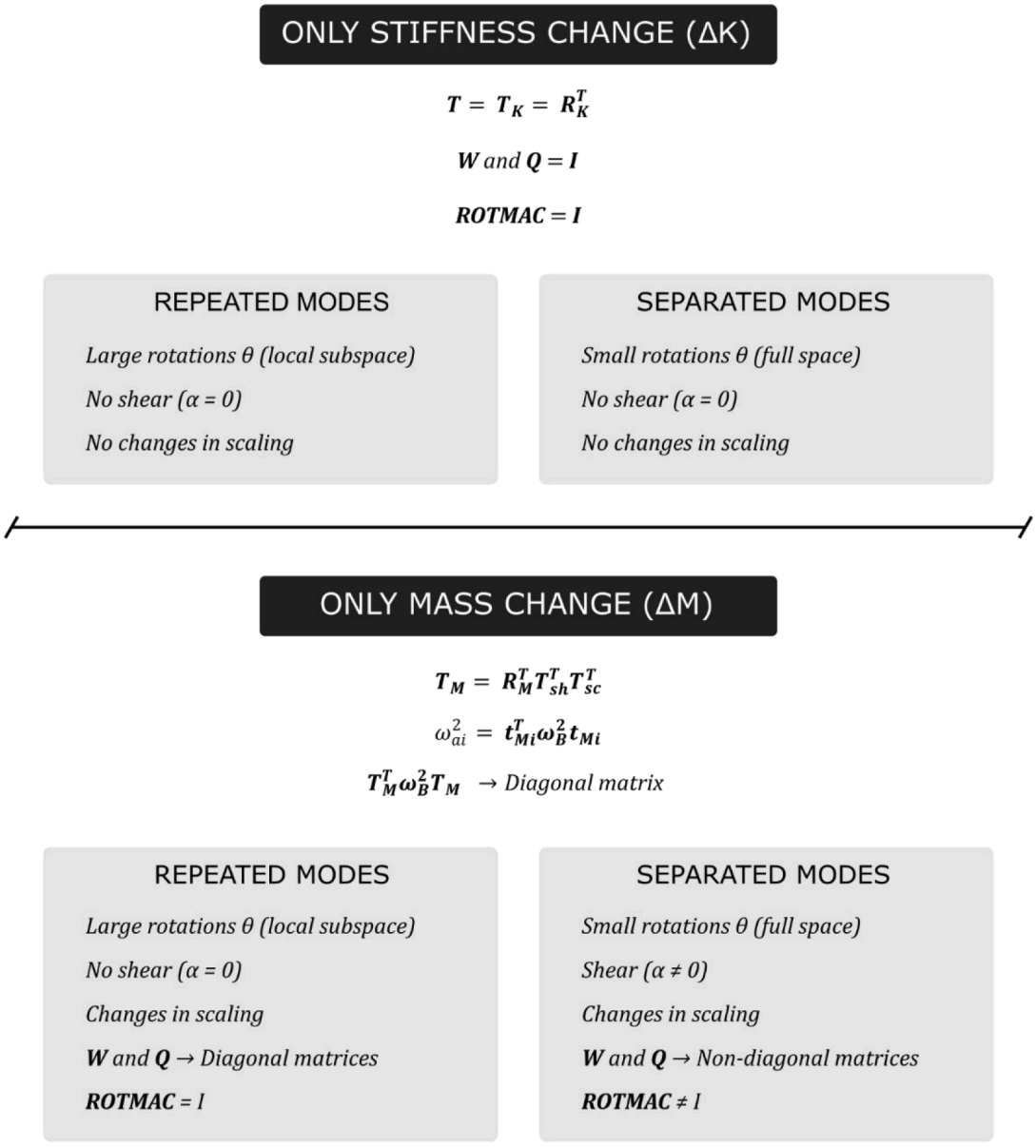

Fig. 3. Main findings presented in this paper in the case of only a stiffness change (ΔK) and only a mass change (ΔM).

software MATLAB [45]. Then the matrix $\boldsymbol{T}$ is factorized with the polar and the QR decompositions, which allow to know the angles of rotation of the mode shapes. The rotated mode shapes of system B are used to calculate the rotated MAC.

Two different models are considered: the first one with separated eigenvalues (section 5.1), and the second one with closely spaced modes (section 5.2).

5.1. 2 DOF system with separated modes

A system B, defined by the following mass and stiffness matrices:

$$\boldsymbol{M_B} = \begin{bmatrix} 2 & 0 \\ 0 & 2 \end{bmatrix}; \boldsymbol{K_B} = \begin{bmatrix} 28 & -12 \\ -12 & 28 \end{bmatrix}$$

has been perturbed with the following mass change and stiffness change matrices:

$$\Delta\boldsymbol{M} = \begin{bmatrix} 0.3 & 0.05 \\ 0.05 & 0.1 \end{bmatrix}; \Delta\boldsymbol{K} = \begin{bmatrix} 3 & -3 \\ -3 & 8 \end{bmatrix}$$

Three different perturbation scenarios have been considered: only mass change defined by the matrix $\Delta\boldsymbol{M}$, only stiffness change defined by the matrix $\Delta\boldsymbol{K}$, and a simultaneous mass and stiffness change $(\Delta\boldsymbol{K} + \Delta\boldsymbol{M})$. The natural frequencies and the mode shapes (normalized to the mass matrix) of both systems are shown in Table 1. It can be observed that this is a system with well-separated eigenvalues.

The MAC between system B and system A is presented in Table 2, where it can be observed that a good correlation, in terms of mode shapes, exists between systems B and A. The best correlation corresponds to system A perturbed with $\Delta\boldsymbol{M}$, whereas the poorest corresponds to system A modified with $\Delta\boldsymbol{K} + \Delta\boldsymbol{M}$. The inner product $\boldsymbol{T^T T}$, which is an identity matrix when there are no discrepancies in terms of mass, is also presented in Table 2. As observed, the diagonal terms of the inner product $\boldsymbol{T^T T}$ indicate a significant change in the scaling of the mode shapes when the structure is perturbed with $\Delta\boldsymbol{M}$ and $\Delta\boldsymbol{K} + \Delta\boldsymbol{M}$, as presented in Table 2.

The matrices $\boldsymbol{T}$ were estimated with Eq. (7), and the matrices $\boldsymbol{T^T}$ were factorized using the left polar decomposition and the QR decomposition. The matrices $\boldsymbol{R}$ and $\boldsymbol{W}$ obtained from the left polar decomposition are presented in Table 3. In this case, the rotation matrix has the format:

$$\boldsymbol{R} = \begin{bmatrix} cos\theta & -sin\theta \\ sin\theta & cos\theta \end{bmatrix} \tag{44}$$

where θ is the angle of rotation. The matrices $\boldsymbol{R}$ and $\boldsymbol{Q}$, along with the angle θ, obtained with the QR decomposition are also presented in Table 3.

From Table 3 it is inferred that a pure rotation is obtained when system B is perturbed with a stiffness change $(\Delta\boldsymbol{K})$, and the same rotation matrix is obtained with the polar and the QR decompositions. The matrices $\boldsymbol{W}$ and $\boldsymbol{Q}$ are identity matrices.

When system B is perturbed with a mass change matrix $(\Delta\boldsymbol{M})$, the rotation matrices obtained with the polar and the QR decompositions are slightly different, leading to different angles of rotation. Moreover, changes in the scaling of the mode shapes and in the relative angle between the mode shapes (shear), can be inferred from matrices $\boldsymbol{W}$ and $\boldsymbol{Q}$. The change in scaling is obtained from the diagonal terms of these matrices, while the shear is derived from the off-diagonal terms.

When system B is perturbed with mass and stiffness $(\Delta\boldsymbol{M} + \Delta\boldsymbol{K})$, the transformation matrix is also decomposed into rotation, scaling and shear, and the results obtained with the polar and the QR decompositions are again slightly different.

The mode shapes of both systems B and A, corresponding to the aforementioned perturbations, are graphically shown in Fig. 4. Moreover, the rotated mode shapes $\boldsymbol{B_R}$ estimated with the polar and QR decompositions are also shown. It can be seen that the mode shapes of system A coincide with the rotated mode shapes when system B is perturbed only with a stiffness change $(\Delta\boldsymbol{K})$. On the other hand, a relative angle exists between mode shapes $\boldsymbol{A}$ and $\boldsymbol{B_R}$ when system B is perturbed with a mass change $(\Delta\boldsymbol{M})$, or a combination of mass and stiffness $(\Delta\boldsymbol{M} + \Delta\boldsymbol{K})$, which depend on the factorization technique. Approximately the same angle α is obtained for the two sets of modes with the polar decomposition, whereas a pair of mode shapes coincide with the QR decomposition and the angle between the other pair of mode shapes is approximately 2α. The relative angles between the mode shapes $\boldsymbol{A}$ and $\boldsymbol{B_R}$ are shown in Table 4.

The ROTMAC between the rotated mode shapes $(\boldsymbol{B_R})$ and the mode shapes of system A is shown in Table 5. As expected, ROTMAC is

Table 1
Natural frequencies and mode shapes of systems A and B.

Mode parameter	System B	System A		
		Perturbation with		
		$\Delta\boldsymbol{K}$	$\Delta\boldsymbol{M}$	$\Delta\boldsymbol{K} + \Delta\boldsymbol{M}$
Mode shapes	$\begin{bmatrix} -0.5 & -0.5 \\ -0.5 & 0.5 \end{bmatrix}$	$\begin{bmatrix} -0.5395 & -0.4571 \\ -0.4571 & 0.5395 \end{bmatrix}$	$\begin{bmatrix} -0.4841 & -0.4479 \\ -0.4571 & 0.5172 \end{bmatrix}$	$\begin{bmatrix} -0.5162 & -0.4105 \\ -0.4172 & 0.5499 \end{bmatrix}$
Natural frequencies ω^2	$\begin{bmatrix} 8 & 0 \\ 0 & 20 \end{bmatrix}$	$\begin{bmatrix} 9.1465 & 0 \\ 0 & 24.3535 \end{bmatrix}$	$\begin{bmatrix} 7.1020 & 0 \\ 0 & 18.6670 \end{bmatrix}$	$\begin{bmatrix} 8.0663 & 0 \\ 0 & 22.8814 \end{bmatrix}$

Table 2
MAC and $\boldsymbol{T}^T\boldsymbol{T}$ between the mode shapes of systems B and A.

System B perturbed with	*MAC*	$\boldsymbol{T}^T\boldsymbol{T}$
$\Delta\boldsymbol{K}$	$\begin{bmatrix} 0.9932 & 0.0068 \\ 0.0068 & 0.9932 \end{bmatrix}$	$\begin{bmatrix} 1.0000 & 0.0000 \\ 0.0000 & 1.0000 \end{bmatrix}$
$\Delta\boldsymbol{M}$	$\begin{bmatrix} 0.9992 & 0.0008 \\ 0.0051 & 0.9949 \end{bmatrix}$	$\begin{bmatrix} 0.8867 & -0.0391 \\ -0.0391 & 0.9362 \end{bmatrix}$
$\Delta\boldsymbol{K} + \Delta\boldsymbol{M}$	$\begin{bmatrix} 0.9889 & 0.0111 \\ 0.0206 & 0.9794 \end{bmatrix}$	$\begin{bmatrix} 0.8811 & -0.0350 \\ -0.0350 & 0.9418 \end{bmatrix}$

Table 3
Left polar and QR decomposition results.

System B perturbed with	Decomposition	Matrix $\boldsymbol{R}$	θ (degrees)	Matrix $\boldsymbol{Q}$ or $\boldsymbol{W}$
$\Delta\boldsymbol{K}$	Polar	$\begin{bmatrix} 0.9966 & 0.0825 \\ -0.0825 & 0.9966 \end{bmatrix}$	−4.7312	$\begin{bmatrix} 1 & 0 \\ 0 & 1 \end{bmatrix}$
	QR	$\begin{bmatrix} 0.9966 & 0.0825 \\ -0.0825 & 0.9966 \end{bmatrix}$	−4.7312	$\begin{bmatrix} 1 & 0 \\ 0 & 1 \end{bmatrix}$
$\Delta\boldsymbol{M}$	Polar	$\begin{bmatrix} 0.9987 & 0.0505 \\ -0.0508 & 0.9987 \end{bmatrix}$	−2.8924	$\begin{bmatrix} 0.9414 & -0.0205 \\ -0.0205 & 0.9674 \end{bmatrix}$
	QR	$\begin{bmatrix} 0.9974 & 0.0716 \\ -0.0716 & 0.9974 \end{bmatrix}$	−4.1065	$\begin{bmatrix} 0.9408 & -0.0404 \\ 0 & 0.9676 \end{bmatrix}$
$\Delta\boldsymbol{K} + \Delta\boldsymbol{M}$	Polar	$\begin{bmatrix} 0.9922 & 0.1249 \\ -0.1249 & 0.9922 \end{bmatrix}$	−7.1772	$\begin{bmatrix} 0.9385 & -0.0183 \\ -0.0183 & 0.9703 \end{bmatrix}$
	QR	$\begin{bmatrix} 0.9896 & 0.1437 \\ -0.1437 & 0.9896 \end{bmatrix}$	−8.2599	$\begin{bmatrix} -0.9380 & 0.0361 \\ 0 & 0.9705 \end{bmatrix}$

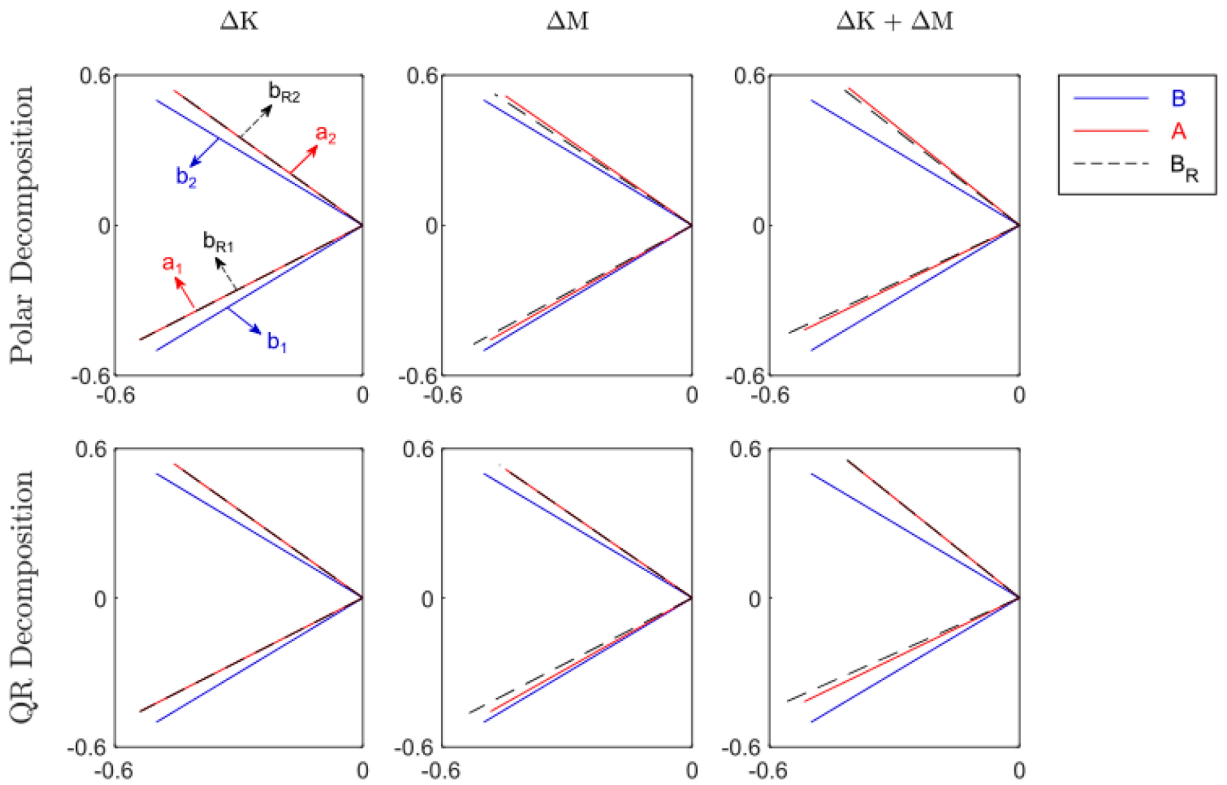

Fig. 4. Modes shapes of system A, B and rotated B in the different perturbation scenarios.

an identity matrix when there are no differences in terms of mass between systems A and B.

In the case of mass discrepancies, the ROTMAC obtained with the polar and the QR decompositions is slightly different. The diagonal terms of ROTMAC are equal and less than unity when the rotation matrix is obtained with the polar decomposition (the angle α

Table 4
Angle α (degrees) between the mode shapes **A** and $\boldsymbol{B_R}$

System B perturbed with	Angle between $\boldsymbol{b}_{R1}$ and $\boldsymbol{a}_1$ (degrees)		Angle between $\boldsymbol{b}_{R2}$ and $\boldsymbol{a}_2$ (degrees)	
	Polar decomp.	QR decomp.	Polar decomp.	QR decomp.
$\Delta\boldsymbol{K}$	0	0	0	0
$\Delta\boldsymbol{M}$	1.2475	2.4615	1.2140	0.0000
$\Delta\boldsymbol{K}+\Delta\boldsymbol{M}$	1.1193	2.2020	1.0827	0.0000

Table 5
Rotated MAC between mode shapes of system A and rotated system B (using the rotation matrices estimated with the polar and QR decompositions).

System B perturbed with	ROTMAC	
	Polar decomp.	QR decomp.
$\Delta\boldsymbol{K}$	$\begin{bmatrix}1 & 0\\ 0 & 1\end{bmatrix}$	$\begin{bmatrix}1 & 0\\ 0 & 1\end{bmatrix}$
$\Delta\boldsymbol{M}$	$\begin{bmatrix}0.9995 & 0.0005\\ 0.0004 & 0.9996\end{bmatrix}$	$\begin{bmatrix}0.9982 & 0.0018\\ 0 & 1\end{bmatrix}$
$\Delta\boldsymbol{K}+\Delta\boldsymbol{M}$	$\begin{bmatrix}0.9996 & 0.0004\\ 0.0004 & 0.9996\end{bmatrix}$	$\begin{bmatrix}0.9985 & 0.0015\\ 0 & 1\end{bmatrix}$

between the two pairs of mode shapes is approximately the same). When using the QR decomposition, a diagonal term of ROTMAC is unity (because a pair of mode shapes coincide), whereas the other component is less than the values resulting from the polar decomposition (because the angle between the other pair of mode shapes is approximately 2α (see Fig. 2).

In order to study the effect of the errors in the components of experimental mode shapes, errors ϵ_A of 1 %, 2 % and 5 % are introduced in the components of the modal matrix A. The new components of the mode shapes were generated with a uniform distribution in the range $[(1-\epsilon_A)\phi,(1+\epsilon_A)\phi]$, where ϕ is a component of a mode shape obtained by solving the eigenvalue problem. A total of one thousand modal matrices of system A were generated, and the factorization of the corresponding transformation matrices $\boldsymbol{T}$ using the polar and QR decompositions provides 1000 angles of rotation (θ). The same process is repeated for each perturbation scenario: $\Delta\boldsymbol{K}$, $\Delta\boldsymbol{M}$ and $\Delta\boldsymbol{K}+\Delta\boldsymbol{M}$. The mean value ($\bar{\theta}$) and standard deviation (σ_θ) of these angles are illustrated in Fig 5. It is inferred that the mean value of the angles is not affected by the random errors in the mode shapes and that the standard deviation increases as the error in the mode shapes increases. When using the polar decomposition, the standard deviation of the angle is $\sigma_\theta=\pm 0.33^0$ for errors in the mode shapes of $\epsilon_A=2\%$, and $\sigma_\theta=\pm 0.85^0$ for $\epsilon_A=5\%$. A higher standard deviation is obtained with the QR decomposition, $\sigma_\theta=\pm 0.46^0$ for errors in the mode shapes $\epsilon_A=2\%$, and $\sigma_\theta=\pm 1.18^0$ for $\epsilon_A=5\%$.

5.2. 2 DOF system with closely spaced modes

A system B defined by the following mass and stiffness matrices:

$$\boldsymbol{M}_{\mathbf{B}}=\begin{bmatrix}2 & 0\\ 0 & 2\end{bmatrix};\boldsymbol{K}_{\mathbf{B}}=\begin{bmatrix}16.01 & -0.01\\ -0.01 & 16.01\end{bmatrix}$$

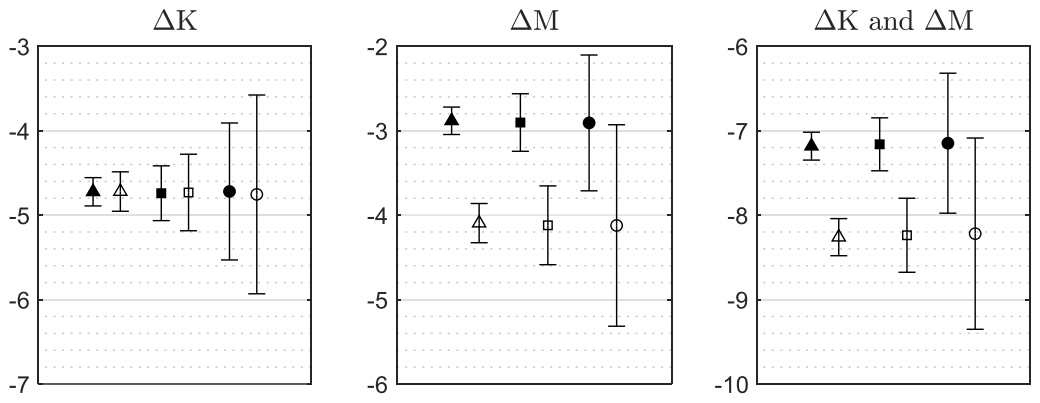

Fig. 5. Mean values of angle θ (degrees) and standard deviation for 1000 simulations with different levels of error in the experimental separated modes shapes: ▲1% error; ■ 2% error; ● 5% error, with both decompositions (full: polar decomposition; empty: QR decomposition).

has been perturbed with the same mass change and stiffness change matrices, i.e:

$$\Delta \boldsymbol{M} = \begin{bmatrix} 0.3 & 0.05 \\ 0.05 & 0.1 \end{bmatrix}; \Delta \boldsymbol{K} = \begin{bmatrix} 3 & -3 \\ -3 & 8 \end{bmatrix}$$

The same perturbation scenarios have been considered: only mass change defined by the matrix $\Delta \boldsymbol{M}$, only stiffness change defined by the matrix $\Delta \boldsymbol{K}$, and a simultaneous mass and stiffness change $(\Delta \boldsymbol{K} + \Delta \boldsymbol{M})$.

The natural frequencies and the mode shapes (normalized to the mass matrix) of both systems are shown in Table 6. It can be observed that this is a system with closely space modes, with a relative frequency shift $\frac{\Delta \omega_b}{\omega_{b1}} = 6.248 \times 10^{-4}$.

The MAC between system B and systems A are presented in Table 7, and MAC values lower than 0.9 have been obtained for all the cases. Concerning the inner product $\boldsymbol{T}^T\boldsymbol{T}$, an identity matrix is obtained when the system is perturbed with a stiffness change $\Delta \boldsymbol{K}$. The diagonal terms of the inner product $\boldsymbol{T}^T\boldsymbol{T}$ indicate a significant change in the scaling of the mode shapes when the structure is perturbed with $\Delta \boldsymbol{M}$ or $\Delta \boldsymbol{M} + \Delta \boldsymbol{K}$.

The matrix $\boldsymbol{T}^T$ was factorized with the left polar decomposition and the QR decomposition, and the corresponding matrices are shown in Table 8. The ROTMAC obtained with both decompositions is presented in Table 9.

Again, the same rotation matrix is obtained with the polar and the QR decompositions when the system is perturbed with a stiffness change $\Delta \boldsymbol{K}$, and the matrices $\boldsymbol{W}$ and $\boldsymbol{Q}$ are identity matrices. Regarding perturbations with a mass matrix ($\Delta \boldsymbol{M}$) and with mass and stiffness ($\Delta \boldsymbol{M} + \Delta \boldsymbol{K}$), the angles of rotation obtained with the polar and the QR decompositions are very close. This results in matrices $\boldsymbol{W}$ and $\boldsymbol{Q}$ being very similar, hence, the same scaling is observed with the polar and QR decompositions, and the effect of shear is minimal. However, the angles of rotation are larger than those obtained for the case of well-separated modes (see Table 3).

The mode shapes of both systems B and A are graphically shown in Figure 6. Once more, the mode shapes of system A coincide with the rotated mode shapes when system B is perturbed only with a stiffness change. When system B is perturbed with a mass change (or a mass and stiffness change $\Delta \boldsymbol{M} + \Delta \boldsymbol{K}$), approximately the same angle α between the two sets of mode shapes is obtained with the polar decomposition. On the other hand, a set of mode shapes coincide with the QR decomposition, whereas an angle of approximately 2α is obtained for the other set of mode shapes.

The ROTMAC between the rotated mode shapes $\boldsymbol{B_R}$ and the mode shapes of system A is shown in Table 9. Once again, ROTMAC is an identity matrix when there are no differences in terms of mass between systems A and B. Regarding cases with mass discrepancies, both the polar and the QR decompositions lead to identity matrices because the modes are closely spaced. However, the diagonal terms of the inner product $\boldsymbol{T}^T\boldsymbol{T}$ (see Table 7), or the matrices $\boldsymbol{W}$ or $\boldsymbol{Q}$, indicate change in the scaling of the mode shapes, i.e., mass discrepancies between both models.

The effect of errors of 1 %, 2 % and 5 % in the components of the experimental mode shapes is shown in Fig 7. The mean value of the angles is not affected by the random errors in the mode shapes, and the standard deviation increases as the error in the mode shapes increases. When using the polar decomposition, the standard deviation of the angle is $\sigma_\theta = \pm 0.25^0$ when the error in the mode shapes is $\epsilon_A = 2\%$, and $\sigma_\theta = \pm 0.64^0$ for $\epsilon_A = 5\%$. A higher standard deviation is obtained with the QR decomposition, $\sigma_\theta = \pm 0.36^0$ when $\epsilon_A = 2\%$, and $\sigma_\theta = \pm 0.92^0$ when $\epsilon_A = 5\%$. From Figs. 5 and 7, it is inferred that a lower scatter has been obtained for the case with closely spaced modes.

6. An experimental case

In this section, the methodology proposed in this paper is applied to correlate a numerical and an experimental model of a square laminated glass plate (Fig. 8). The plate, measuring 1400x1400 mm, consists of two 4 mm thick glass layers and a 1.14 mm polymeric interlayer, and it is pinned supported at the four corners.

The modal parameters were estimated using operational modal analysis (OMA). The structure was excited by applying hits on the plate, randomly in time and space, using an impact hammer. The response of the structure was measured in 25 DOF's using 16 accelerometers with a sensitivity of 100 mV/g and recorded with a TEAC LX-120 data recorder. Two data sets were used to cover the 25 DOF's, and 7 accelerometers were employed as reference sensors (see Fig. 9). A sampling rate of 2000 Hz and an acquisition time of 6 min were utilized.

The modal parameters of the first five modes were estimated with the EFDD (enhanced frequency domain decomposition) technique, and the natural frequencies are shown in Table 10. As it can be seen in Table 10, experimental modes 2 and 3 are closely spaced with relative frequency shift $\frac{\Delta \omega_a}{\omega_a} = 0.0107$. The mode shapes normalized to the unit length are presented in Fig. 10.

Table 6
Natural frequencies and mode shapes of systems A and B.

Mode parameter	System B	System A Perturbation with $\Delta \boldsymbol{K}$	System A Perturbation with $\Delta \boldsymbol{M}$	System A Perturbation with $\Delta \boldsymbol{K} + \Delta \boldsymbol{M}$
Mode shapes	$\begin{bmatrix} -0.5 & -0.5 \\ -0.5 & 0.5 \end{bmatrix}$	$\begin{bmatrix} -0.6401 & -0.3004 \\ -0.3004 & 0.6401 \end{bmatrix}$	$\begin{bmatrix} -0.6392 & -0.1625 \\ -0.1548 & 0.6727 \end{bmatrix}$	$\begin{bmatrix} -0.6060 & -0.2603 \\ -0.2579 & 0.6403 \end{bmatrix}$
Natural frequencies ω^2	$\begin{bmatrix} 8 & 0 \\ 0 & 8.01 \end{bmatrix}$	$\begin{bmatrix} 8.7986 & 0 \\ 0 & 12.7114 \end{bmatrix}$	$\begin{bmatrix} 6.9234 & 0 \\ 0 & 7.6691 \end{bmatrix}$	$\begin{bmatrix} 7.6377 & 0 \\ 0 & 12.1334 \end{bmatrix}$

Table 7
MAC and inner product $\boldsymbol{T}^T\boldsymbol{T}$ between systems A and B.

System B perturbed with	*MAC*	$\boldsymbol{T}^T\boldsymbol{T}$
$\Delta\boldsymbol{K}$	$\begin{bmatrix}0.8846 & 0.1154\\ 0.1154 & 0.8846\end{bmatrix}$	$\begin{bmatrix}1.0000 & 0.0000\\ 0.0000 & 1.0000\end{bmatrix}$
$\Delta\boldsymbol{M}$	$\begin{bmatrix}0.7287 & 0.2713\\ 0.2718 & 0.7282\end{bmatrix}$	$\begin{bmatrix}0.8651 & -0.0005\\ -0.0005 & 0.9578\end{bmatrix}$
$\Delta\boldsymbol{K}+\Delta\boldsymbol{M}$	$\begin{bmatrix}0.8603 & 0.1397\\ 0.1511 & 0.8489\end{bmatrix}$	$\begin{bmatrix}0.8675 & -0.0148\\ -0.0148 & 0.9553\end{bmatrix}$

Table 8
Left polar decomposition and QR decomposition results.

System B perturbed with	Decomposition	Matrix $\boldsymbol{R}$	θ (degrees)	Matrix $\boldsymbol{Q}$ or $\boldsymbol{Z}$
$\Delta\boldsymbol{K}$	Polar	$\begin{bmatrix}0.9405 & 0.3397\\ -0.3397 & 0.9405\end{bmatrix}$	−19.8559	$\begin{bmatrix}1 & 0\\ 0 & 1\end{bmatrix}$
	QR	$\begin{bmatrix}0.9405 & 0.3397\\ -0.3397 & 0.9405\end{bmatrix}$	−19.8559	$\begin{bmatrix}1 & 0\\ 0 & 1\end{bmatrix}$
$\Delta\boldsymbol{M}$	Polar	$\begin{bmatrix}0.8535 & 0.5211\\ -0.5211 & 0.8535\end{bmatrix}$	−31.4047	$\begin{bmatrix}0.9301 & -0.0002\\ -0.0002 & 0.9787\end{bmatrix}$
	QR	$\begin{bmatrix}0.8534 & 0.5213\\ -0.5213 & 0.8534\end{bmatrix}$	−31.4202	$\begin{bmatrix}0.9301 & -0.0005\\ 0.0000 & 0.9787\end{bmatrix}$
$\Delta\boldsymbol{K}+\Delta\boldsymbol{M}$	Polar	$\begin{bmatrix}0.9244 & 0.3815\\ -0.3815 & 0.9244\end{bmatrix}$	−22.4244	$\begin{bmatrix}0.9314 & -0.0077\\ -0.0077 & 0.9774\end{bmatrix}$
	QR	$\begin{bmatrix}0.9213 & 0.3888\\ -0.3888 & 0.9213\end{bmatrix}$	−22.8778	$\begin{bmatrix}0.9313 & -0.0151\\ 0.0000 & 0.9774\end{bmatrix}$

Additionally, a 3D finite element model of the structure was assembled in ANSYS and meshed with 19,200 elements SOLID186 (20-node structural solid elements) and 97,767 nodes. The numerical natural frequencies corresponding to the first 5 modes are shown in Table 10. In this case, modes 2 and 3 are repeated modes.

In operational modal analysis, the mode shapes cannot be mass-normalized; hence, an experimental modal matrix $\boldsymbol{A}_U$ size 25 x 25, containing mode shapes normalized to the unit length, was used. Moreover, to calculate the MAC and to apply Eq. (7), a mass-normalized numerical modal matrix B size 25 x 5 was extracted from the finite element model.

The discrepancies in natural frequencies between both models are less than 9.22 % (see Table 10). The MAC between the mode shapes of the numerical and the experimental models is shown in Table 11, where it can be observed that a good correlation exists for modes 1, 4 and 5, whereas low values of MAC have been obtained for modes 2 and 3.

An estimation of matrix $\boldsymbol{T}_U$ was obtained with the expression:

$$\widehat{\boldsymbol{T}}_U = \boldsymbol{B}^{+}\boldsymbol{A}_U \tag{45}$$

where the superscript '+' indicates pseudoinverse. The left polar and QR decompositions were applied to factorize matrix $\widehat{\boldsymbol{T}}_U^T$. As demonstrated in Appendix D, the QR decomposition provides the same rotation matrix with matrices $\boldsymbol{T}$ (estimated with both numerical and experimental mode shapes mass-normalized) and $\boldsymbol{T}_U$ (estimated with mass-normalized numerical mode shapes and unscaled experimental mode shapes), but this is not the case with the polar decomposition. However, in this section, both factorizations have been used to decompose matrix $\boldsymbol{T}_U$ for comparison purposes. The rotation matrices $\boldsymbol{R}$ obtained with both decompositions are shown in Tables 12 and 13, respectively, whereas matrices $\boldsymbol{W}$ and $\boldsymbol{Q}$ are shown in Tables 14 and 15.

From the matrices $\boldsymbol{R}$ presented in Tables 12 and 13, a rotation angle (θ) of -42.3473° was obtained with polar decomposition and -45.5890° with QR decomposition. The second and third rotated numerical mode shapes are shown in Fig 11, where a good correlation can be observed between both models.

The rotated MAC obtained with the rotation matrices provided by the polar and QR factorizations are presented in Tables 16 and 17, respectively. The matrices are closer to identity which is an indicator of a good correlation (in terms of mass) between both models.

When a truncated modal model is used to estimate the matrix $\boldsymbol{T}_U$, the lasts columns are estimated with less accuracy because of truncation. This explains why the last diagonal term in Tables 16 and 17 is below 0.99. Moreover, the errors in the components of the mode shapes also affects the terms of matrix $\boldsymbol{T}_U$, which means that a pure identity ROTMAC matrix is difficult to achieve in real practice.

7. Conclusions

In several applications of structural dynamics, a system A can be considered a perturbation of a system B. According to structural dynamic modification theory, the mode shapes of a system A (perturbed) can be expressed as a linear combination of the mode shapes of system B (unperturbed) through a transformation matrix $\boldsymbol{T}$. It has been demonstrated that this matrix $\boldsymbol{T}$ can be factorized into a

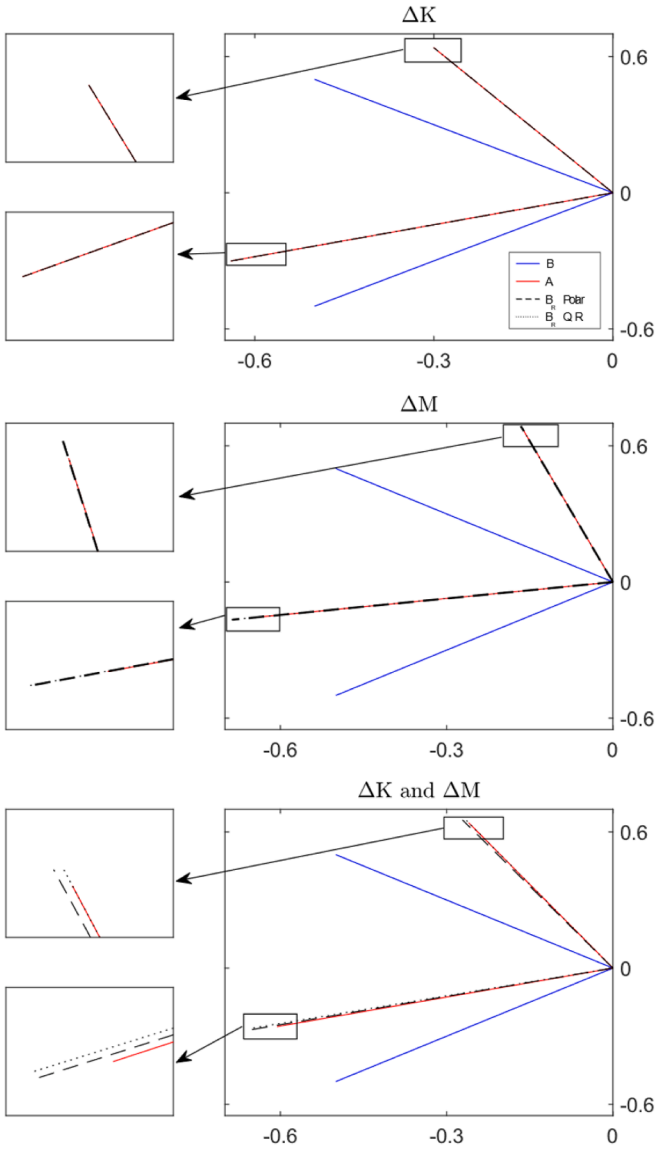

Fig. 6. Modes shapes of system A, B and rotated B in the different perturbation scenarios.

Table 9
ROTMAC between systems A and B.

System B perturbed with	ROTMAC	
	Polar decomp.	QR decomp.
$\Delta \boldsymbol{K}$	$\begin{bmatrix} 1 & 0 \\ 0 & 1 \end{bmatrix}$	$\begin{bmatrix} 1 & 0 \\ 0 & 1 \end{bmatrix}$
$\Delta \boldsymbol{M}$	$\begin{bmatrix} 1 & 0 \\ 0 & 1 \end{bmatrix}$	$\begin{bmatrix} 1 & 0 \\ 0 & 1 \end{bmatrix}$
$\Delta \boldsymbol{K} + \Delta \boldsymbol{M}$	$\begin{bmatrix} 0.9999 & 0.0001 \\ 0.0001 & 0.9999 \end{bmatrix}$	$\begin{bmatrix} 0.9997 & 0.0003 \\ 0 & 1 \end{bmatrix}$

product of two matrices, one of them being a rotation matrix, using the polar and QR decompositions. This factorization becomes a powerful tool for determining whether discrepancies between two models can be attributed to differences in stiffness, mass, or both.

In the case of no mass discrepancies between systems B and A, it has been demonstrated that the inner product $\boldsymbol{T}^T\boldsymbol{T}$ is an identity matrix, meaning that matrix $\boldsymbol{T}$ is a rotation matrix. In this case, the factorization using both polar and QR decompositions yields the

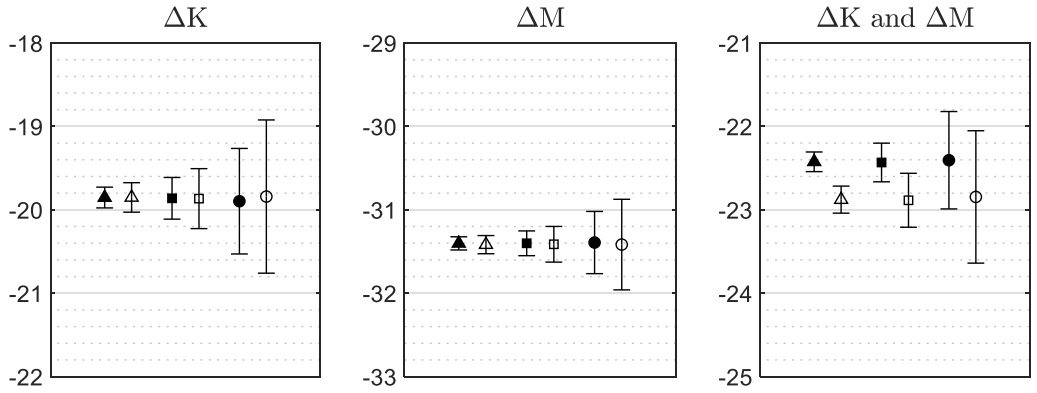

Fig. 7. Mean values of angle θ (degrees) and standard deviation for 1000 simulations with different levels of error in the experimental closely spaced modes shapes: ▲1% error; ■ 2% error; ● 5% error, with both decompositions (full: polar decomposition; empty: QR decomposition).

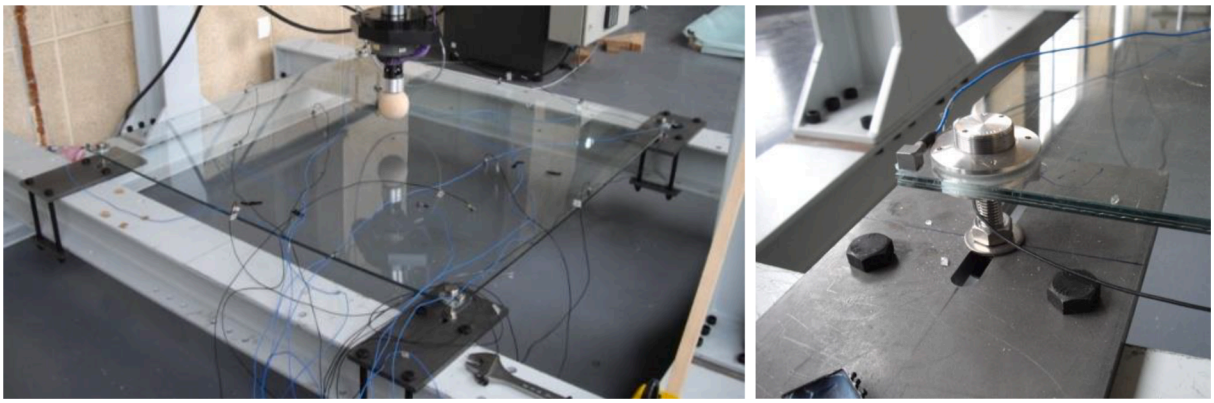

Fig. 8. Square laminated glass plate.

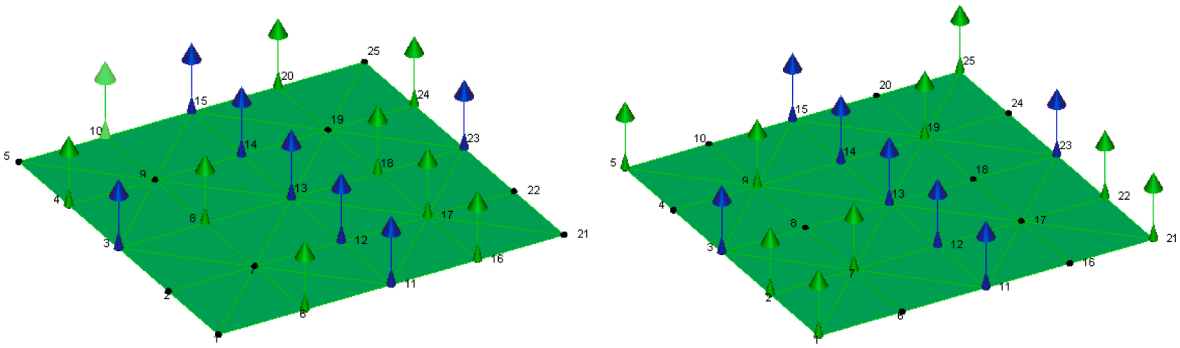

Fig. 9. Test setup for the two data sets.

same rotation matrix, and the matrices $\boldsymbol{W}$ are $\boldsymbol{Q}$ are identity matrices. This indicates that the scaling and the relative angle between mode shapes are not modified. The angle of rotation is small when the modes of the system are well-separated, affecting the full set of modes. Conversely, larger angles can be obtained when the system presents closely spaced or repeated modes, but the effect is mainly limited to a local rotation in the subspace defined by the closely or repeated modes.

In the case of mass discrepancies between systems B and A, the inner product $\boldsymbol{T}_{\boldsymbol{M}}^{T}\boldsymbol{\omega}_{\boldsymbol{B}}^{2}\boldsymbol{T}_{\boldsymbol{M}}$ must result in a diagonal matrix, and the natural frequencies of systems B and A are related as $\omega_{ai}^{2} = \boldsymbol{t}_{\boldsymbol{Mi}}^{T}\boldsymbol{\omega}_{\boldsymbol{B}}^{2}\boldsymbol{t}_{\boldsymbol{Mi}}$. The factorization of matrix $\boldsymbol{T}$ provides matrices $\boldsymbol{W}$ and $\boldsymbol{Q}$, where the diagonal terms contain information about the changes in scaling and the off-diagonal terms contain information about the shear. However, the polar and QR factorizations yield different shear effects, resulting in two different solutions, i.e. the rotation matrices obtained with the polar and the QR decompositions are slightly different.

Table 10
Experimental and numerical natural frequencies.

Mode Shapes	Natural frequencies [Hz]		Error [%]
	Experimental (Model A)	Numerical (Model B)	
Mode 1	9.35	9.72	3.80
Mode 2	19.62	21.11	7.01
Mode 3	19.83	21.11	6.10
Mode 4	22.53	24.82	9.22
Mode 5	55.76	56.11	0.62

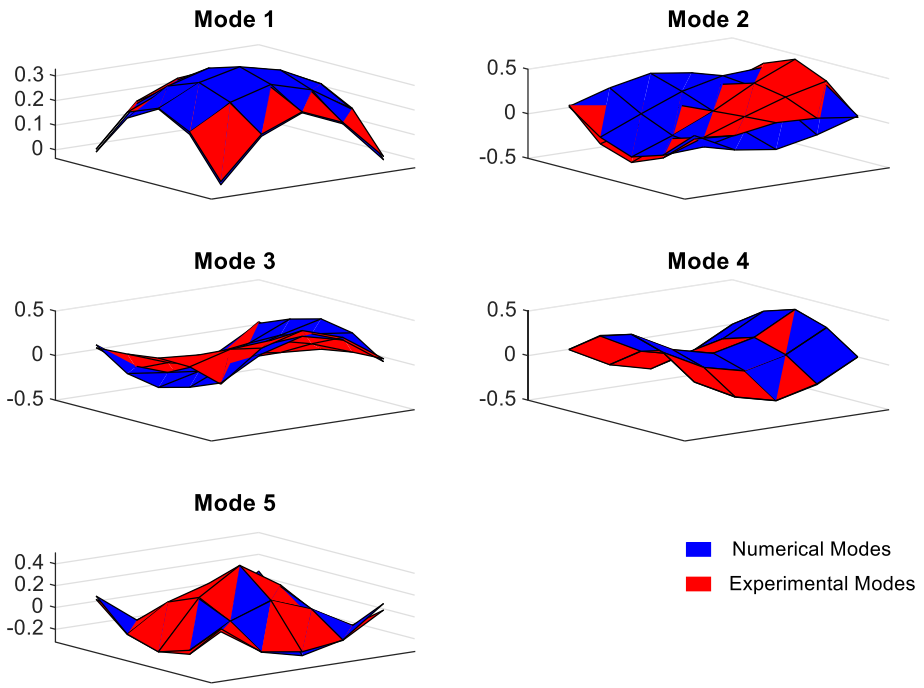

Fig. 10. Numerical and experimental mode shapes normalized to the unit length.

Table 11
Modal assurance criterion for numerical and experimental mode shapes.

MAC				
0.9971	0.0000	0.0001	0.0000	0.0976
0.0000	0.5990	0.3965	0.0000	0.0001
0.0000	0.5088	0.4896	0.0002	0.0000
0.0000	0.0001	0.0000	0.9996	0.0000
0.0661	0.0002	0.0007	0.0000	0.9862

Table 12
Rotation matrix $\boldsymbol{R}$ obtained with left polar decomposition.

0.9996	−0.0025	−0.0039	−0.0007	−0.0291
0.0042	0.7390	0.6736	0.0052	−0.0110
0.0010	−0.6736	0.7390	−0.0111	−0.0072
−0.0007	0.0113	−0.0047	−0.9999	0.0008
0.0292	0.0032	0.0126	0.0008	0.9995

In the case of both mass and stiffness discrepancies, the factorization of matrix $\boldsymbol{T}$ provides a rotation matrix which can be decomposed into a product of two rotation matrices due to mass and stiffness, respectively.

If the mode shapes of system A are not mass-normalized, a different transformation matrix $\boldsymbol{T}_U$ is obtained. It has been demonstrated

Table 13
Rotation matrix $\boldsymbol{R}$ obtained with QR decomposition.

−0.9992	0.0068	−0.0006	0.0008	0.0390
−0.0031	−0.6997	−0.7137	−0.0050	0.0330
0.0056	0.7141	−0.6998	0.0109	0.0084
0.0007	−0.0113	0.0040	0.9999	−0.0004
−0.0391	−0.0168	−0.0295	−0.0005	−0.9987

Table 14
$\boldsymbol{W}$matrix obtained with left polar decomposition.

1.4821	0.0007	−0.0075	0.0001	0.0104
0.0007	1.1904	−0.0675	0.0005	0.0228
−0.0075	−0.0675	1.1973	0.0004	0.0035
0.0001	0.0005	0.0004	0.9801	0.0004
0.0104	0.0228	0.0035	0.0004	1.0593

Table 15
$\boldsymbol{Q}$ matrix obtained with QR decomposition.

−1.4819	0.0007	0.0168	−0.0001	−0.0249
0.0000	−1.1840	0.1345	−0.0011	−0.0482
0.0000	0.0000	−1.1992	−0.0009	−0.0060
0.0000	0.0000	0.0000	−0.9801	−0.0007
0.0000	0.0000	0.0000	0.0000	−1.0596

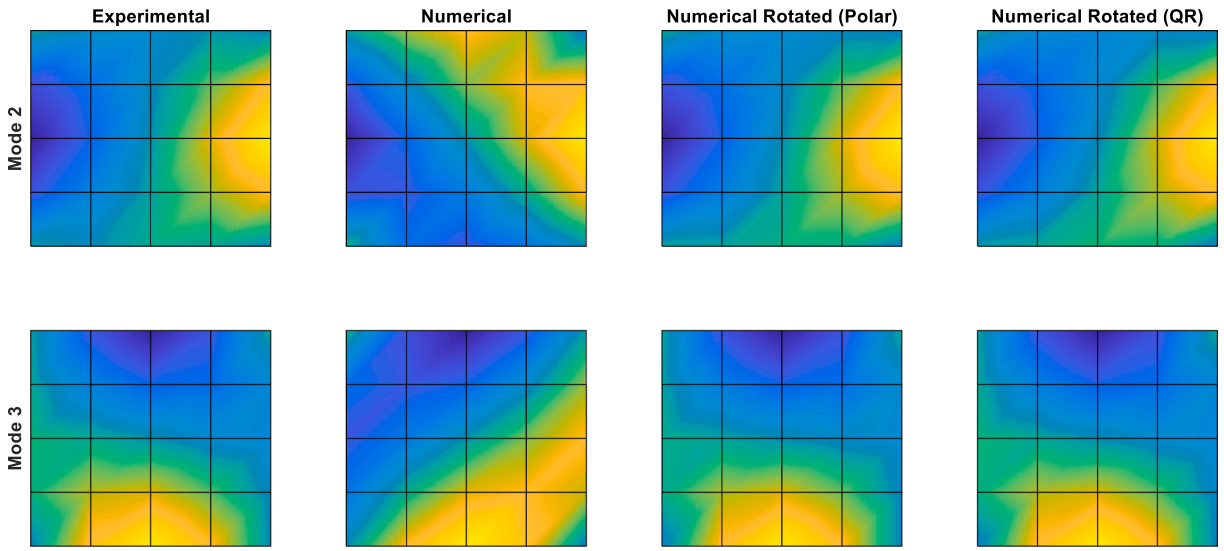

Fig. 11. Experimental and numerical (before and after rotation) modes 2 and 3.

Table 16
Rotated MAC with left polar decomposition.

0.9980	0.0000	0.0000	0.0000	0.0860
0.0000	0.9921	0.0031	0.0000	0.0003
0.0000	0.0031	0.9954	0.0000	0.0000
0.0000	0.0000	0.0000	0.9997	0.0000
0.0865	0.0002	0.0000	0.0000	0.9874

that the QR decomposition of matrices $\boldsymbol{T}$ and $\boldsymbol{T}_U$ provides the same rotation matrix. However, different rotation matrices are obtained by factorizing matrices $\boldsymbol{T}$ and $\boldsymbol{T}_U$ with the polar decomposition.

Since the rotation of the mode shapes does not modify the mass matrix of a system, this paper introduces a novel and physically

Table 17
Rotated MAC with QR decomposition.

0.9974	0.0001	0.0001	0.0000	0.0822
0.0000	0.9810	0.0125	0.0000	0.0013
0.0000	0.0000	0.9986	0.0000	0.0000
0.0000	0.0000	0.0000	0.9997	0.0000
0.0938	0.0001	0.0000	0.0000	0.9879

meaningful version of the modal assurance criterion, denoted as Rotated MAC or ROTMAC. With this definition, the mode shapes of system B must be rotated using the rotation matrices identified with the factorization techniques used in this paper, and then correlated with the mode shapes of system A. The ROTMAC, combined with the diagonal terms of the inner product $\boldsymbol{T}^T\boldsymbol{T}$, can be used to detect differences in terms of mass between two models.

The equations and the conclusions derived in this paper have been validated through numerical simulations and an experimental test. Firstly, the methodology was validated by numerical simulations of a 2 DOF system considering two different scenarios: a case with well-separated modes and another with closely spaced modes. As expected, larger angles of rotation were obtained for the case with closely spaced modes. The mode shapes of system B have the same length, and consequently, approximately the same angle α between the two sets of mode shapes is obtained with the polar decomposition. With respect to the QR decomposition, a set of mode shapes coincide, whereas approximately an angle 2α is obtained for the other set of mode shapes. Moreover, it has been proven that the ROTMAC is an identity matrix when there are no differences in terms of mass between systems A and B.

Then, a numerical and an experimental model of a square laminated glass plate were correlated. The first five experimental mode shapes were estimated with operational modal analysis, and two data sets were used to cover 25 DOF's. The same number of modes and DOF's were considered in the numerical model. The numerical mode shapes were normalized to the mass of the system, whereas the experimental mode shapes were normalized to the unit length. Both QR and polar decompositions were used to factorize matrix $\boldsymbol{T}_U$. The classical MAC revealed a poor correlation between the second and the third modes, which were repeated in the numerical model and closely spaced in the experimental model. However, through the factorization of the $\boldsymbol{T}$ matrix and the calculation of the rotated MAC, it was confirmed that a good correlation in terms of mass exists between both models. In this case, the rotation is limited to the subspace spanned by the closely spaced modes.

CRediT authorship contribution statement

M. Aenlle: Writing – review & editing, Writing – original draft, Supervision, Project administration, Investigation, Funding acquisition, Conceptualization. **N. García-Fernández:** Writing – review & editing, Writing – original draft, Validation, Software, Methodology, Formal analysis. **F. Pelayo:** Funding acquisition, Writing – original draft, Writing – review & editing, Methodology, Project administration.

Declaration of competing interest

The authors declare that they have no known competing financial interests or personal relationships that could have appeared to influence the work reported in this paper.

Data availability

Data will be made available on request.

Acknowledgements

This work was supported by the Spanish Ministry of Science and Innovation [MCI-20-PID2019-105593 GB-I00/AEI/10.13039/501100011033 and MCI-21-PRE2020-094923].

APPENDIX A. DECOMPOSTION OF MATRIX T FOR A MASS PERTURBATION

The effects of a mass change perturbation can also be demonstrated particularizing Eq. (19) for a system with two modes, which leads to:

$$\begin{bmatrix} \omega_{a1}^2 & 0 \\ 0 & \omega_{a2}^2 \end{bmatrix} = \begin{bmatrix} t_{11}^2\omega_{b1}^2 + t_{21}^2\omega_{b2}^2 & t_{11}\omega_{b1}^2 t_{12} + t_{21}\omega_{b2}^2 t_{22} \\ t_{11}\omega_{b1}^2 t_{12} + t_{21}\omega_{b2}^2 t_{22} & t_{12}^2\omega_{b1}^2 + t_{22}^2\omega_{b2}^2 \end{bmatrix} \tag{A1}$$

From Eq. (A1) it is derived that:

$$\frac{t_{11}}{t_{21}} = -\frac{t_{22}}{t_{12}}\frac{\omega_{b2}^2}{\omega_{b1}^2} \tag{A2}$$

And:

$$\frac{t_{12}}{t_{21}} = -\frac{\omega_{a2}}{\omega_{a1}}\frac{\omega_{b2}}{\omega_{b1}}\frac{t_{11}}{t_{22}} = \frac{\omega_{a1}}{\omega_{a2}}\frac{\omega_{b2}}{\omega_{b1}} \tag{A3}$$

Using the results of Eq. (A2) and Eq. (A3), the matrix $\boldsymbol{T_M}$ can be expressed as:

$$\boldsymbol{T_M} = \begin{bmatrix} t_{11} & -\frac{\omega_{a2}}{\omega_{a1}}\sqrt{\left(\frac{\omega_{a1}^2}{\omega_{b1}^2} - t_{11}^2\right)} \\ \frac{\omega_{b1}}{\omega_{b2}}\sqrt{\left(\frac{\omega_{a1}^2}{\omega_{b1}^2} - t_{11}^2\right)} & t_{11}\frac{\omega_{a2}}{\omega_{a1}}\frac{\omega_{b1}}{\omega_{b2}} \end{bmatrix} \tag{A4}$$

From Eq. (A4), it is inferred that the inner product $\boldsymbol{T_M^T T_M}$ must be a diagonal matrix if $\omega_{b1} = \omega_{b2}$ (repeated modes), i.e., there is no effect of shear. Moreover, matrix $\boldsymbol{T_M}$ becomes a pure rotation if $\omega_{b1} = \omega_{b2}$ (repeated modes), and $\omega_{a1} = \omega_{a2} = \omega_{b1} = \omega_{b2}$, i.e., when $\Delta \boldsymbol{M} \rightarrow 0$.

Thus, in the case of repeated or closely spaced modes, the effect of a mass change is mainly a rotation of the mode shapes (in the local subspace defined by the closely or repeated modes) and a change in scaling. The angle of rotation of the mode shapes is maximum for repeated modes, and it decreases as the frequency shift $\Delta\omega_b = \omega_{b2} - \omega_{b1}$ increases. Additionally, the effect of shear is negligible for repeated modes, and it increases as the frequency shift $\Delta\omega_b$ increases.

APPENDIX B. POLAR and QR DECOMPOSITIONS OF MATRIX T

The right polar decomposition [30–32,41] of a real matrix $\boldsymbol{P}$ size $\boldsymbol{m} \times \boldsymbol{n}$ $(\boldsymbol{m} \geq \boldsymbol{n})$ is a factorization of the form:

$$\boldsymbol{P} = \boldsymbol{RZ} \tag{B1}$$

where matrix $\boldsymbol{R}$ is also size $\boldsymbol{m} \times \boldsymbol{n}$ and with orthogonal columns, i.e. $\boldsymbol{R^T R} = \boldsymbol{I_n}$ where $\boldsymbol{I_n}$ denotes the identity matrix of order $\boldsymbol{n}$. $\boldsymbol{Z}$ is a positive semi-definite Hermitian matrix. If $\boldsymbol{P^T P}$ has no negative real eigenvalues, the decomposition is unique.

If $\boldsymbol{P}$ is a real square non-singular matrix $(\boldsymbol{m} = \boldsymbol{n})$, matrix $\boldsymbol{R}$ is orthogonal $(\boldsymbol{R^T R} = \boldsymbol{RR^T} = \boldsymbol{I_n})$, i.e. it is a rotation matrix when $det(\boldsymbol{T^T}) > 0$ or a reflection when $det(\boldsymbol{T^T}) < 0$ [42]. The polar decomposition of a square matrix $\boldsymbol{P}$ always exists. If $\boldsymbol{P}$ is invertible, the decomposition is unique, and $\boldsymbol{W}$ will be positive-definite.

On the other hand, the left polar decomposition [30–32,41] of a real matrix $\boldsymbol{P}$ (size $\boldsymbol{m} \times \boldsymbol{n}$) is a factorization of the form:

$$\boldsymbol{P} = \boldsymbol{WR} \tag{B2}$$

where matrix $\boldsymbol{R}$ is also size $\boldsymbol{m} \times \boldsymbol{n}$ and has orthogonal columns, and $\boldsymbol{W}$ is a positive semi-definite hermitian matrix. If $\boldsymbol{P}$ is a real square non-singular matrix $(\boldsymbol{m} = \boldsymbol{n})$, matrix $\boldsymbol{R}$ is a rotation matrix or a reflection matrix.

The matrices $\boldsymbol{Z}$ and $\boldsymbol{W}$ can be obtained by means of the following equations [30–32,41]:

$$\boldsymbol{Z} = \left(\boldsymbol{P^T P}\right)^{1/2} \tag{B3}$$

$$\boldsymbol{W} = \left(\boldsymbol{PP^T}\right)^{1/2} \tag{B4}$$

The matrices $\boldsymbol{W}$ and $\boldsymbol{R}$ (or $\boldsymbol{R}$ and $\boldsymbol{Z}$) can also be obtained decomposing the inner product $\boldsymbol{T^T T}$ in singular values, i.e.:

$$\boldsymbol{P^T P} = \boldsymbol{USV^T} \tag{B5}$$

where matrix $\boldsymbol{S}$ contains the singular values, and matrices $\boldsymbol{U}$ and $\boldsymbol{V}$ contain the singular vectors. Matrix $\boldsymbol{W}$ is obtained from Eq. (B5) [30,31] as:

$$\boldsymbol{W} = \boldsymbol{V}\sqrt{\boldsymbol{S}}\boldsymbol{V^T} \tag{B6}$$

And matrix $\boldsymbol{R}$ as:

$$\boldsymbol{R} = \boldsymbol{PZ}^{-1} \tag{B7}$$

The right polar decomposition can be used to factorize matrix $\boldsymbol{T^T}$ as:

$$\boldsymbol{T^T} = \boldsymbol{R}_1\boldsymbol{Z}_1 \tag{B8}$$

or matrix $\boldsymbol{T}$ as:

$$\boldsymbol{T} = \boldsymbol{R}_2\boldsymbol{Z}_2 \tag{B9}$$

On the other hand, the left polar decomposition [41] factorizes matrix $\boldsymbol{T^T}$ as:

$$\boldsymbol{T^T} = \boldsymbol{W}_1\boldsymbol{R}_1 \tag{B10}$$

or matrix $\boldsymbol{T}$ as:

$$\boldsymbol{T} = \boldsymbol{W}_2\boldsymbol{R}_2 \tag{B11}$$

From Eqs. (B8-B11), it is derived that:

$$\boldsymbol{R}_2 = \boldsymbol{R}_1^T \tag{B12}$$

$$\boldsymbol{Z}_2 = \boldsymbol{W}_1^T \tag{B13}$$

$$\boldsymbol{W}_2 = \boldsymbol{Z}_1^T \tag{B14}$$

It is worth emphasizing that the transpose of a rotation matrix is also a rotation matrix.

The QR decomposition [33–35] of a matrix $\boldsymbol{P}$ size $\boldsymbol{m} \times \boldsymbol{n}$ $(\boldsymbol{m} \geq \boldsymbol{n})$ is a factorization of the form:

$$\boldsymbol{P} = \boldsymbol{R}\boldsymbol{Q} \tag{B15}$$

Where matrix $\boldsymbol{R}$ is size $\boldsymbol{m} \times \boldsymbol{m}$, it has orthogonal columns and $\boldsymbol{R}^T\boldsymbol{R} = \boldsymbol{I}_m$. If $\boldsymbol{P}$ is full rank, the QR decomposition always exists but, in general, is not unique.

If matrix $\boldsymbol{P}$ is square size $\boldsymbol{n} \times \boldsymbol{n}$, matrix $\boldsymbol{R}$ is orthogonal ($\boldsymbol{R}^T\boldsymbol{R} = \boldsymbol{R}\boldsymbol{R}^T = \boldsymbol{I}_n$), i.e. it is rotation matrix. If matrix $\boldsymbol{P}$ is invertible, then the factorization is unique.

Using the QR decomposition, matrix $\boldsymbol{T}^T$ can be factorized as:

$$\boldsymbol{T}^T = \boldsymbol{R}_1\boldsymbol{Q}_{1a} \tag{B16}$$

And matrix $\boldsymbol{T}$ as:

$$\boldsymbol{T} = \boldsymbol{R}_2\boldsymbol{Q}_{2a} \tag{B17}$$

On the other hand, the RQ decomposition gives:

$$\boldsymbol{T}^T = \boldsymbol{Q}_{1b}\boldsymbol{R}_1 \tag{B18}$$

And

$$\boldsymbol{T} = \boldsymbol{Q}_{2b}\boldsymbol{R}_2 \tag{B19}$$

From Eqs. (B9) and (B17), it is inferred that the rotation matrices obtained with the polar ($\boldsymbol{R}_{2(Polar)}$) and the QR decompositions ($\boldsymbol{R}_{2(QR)}$) are related by the equation:

$$\boldsymbol{R}_{2(QR)} = \boldsymbol{R}_{2(Polar)}\,\boldsymbol{Z}_2\,\boldsymbol{Q}_{2a}^{-1} \tag{B20}$$

APPENDIX C. DIFFERENCES BEWTEEN POLAR AND QR DECOMPOSTIONS

Using Eq. (B9), matrix $\boldsymbol{T}$ is expressed as:

$$\boldsymbol{T} = \boldsymbol{R}_2\boldsymbol{Z}_2 \tag{C1}$$

In a system with two DOF's and two modes, Eq. (C1) is given by:

$$[\boldsymbol{t}_1\,\boldsymbol{t}_2] = [\boldsymbol{r}_1\,\boldsymbol{r}_2]\begin{bmatrix} z_{11} & z_{12} \\ z_{21} & z_{22} \end{bmatrix} \tag{C2}$$

Where $\boldsymbol{t}_1$ and $\boldsymbol{t}_2$ are two column vectors of matrix $\boldsymbol{T}$, $\boldsymbol{r}_1$ and $\boldsymbol{r}_2$ are two column vectors of matrix $\boldsymbol{R}_2$, and $z_{12} = z_{21}$.

The vectors $\boldsymbol{r}_1$ and $\boldsymbol{r}_2$ are orthogonal, and they are the vectors closer to $\boldsymbol{t}_1$ and $\boldsymbol{t}_2$, which means that the angle γ between the vectors of matrix $\boldsymbol{T}$ and the vectors of matrix $\boldsymbol{R}_2$ is minimum (see Fig. 2).

The mode shapes of system A can be expressed as linear combination of the rotated unperturbed mode shapes as:

$$\boldsymbol{A} = \boldsymbol{B}\,\boldsymbol{T} = \boldsymbol{B}\,\boldsymbol{R}_2\,\boldsymbol{Z}_2 \tag{C3}$$

Substitution of Eq. (B12) in Eq. (C3) gives:

$$\boldsymbol{A} = \boldsymbol{B}\,\boldsymbol{R}_1^T\,\boldsymbol{Z}_2 = \boldsymbol{B}_R\,\boldsymbol{Z}_2 \tag{C4}$$

or

$$[\boldsymbol{a}_1\,\boldsymbol{a}_2] = [\boldsymbol{b}_{R1}\,\boldsymbol{b}_{R2}]\begin{bmatrix} z_{11} & z_{12} \\ z_{21} & z_{22} \end{bmatrix} \tag{C5}$$

If the length of the mode shapes $\boldsymbol{b}_{R1}$ and $\boldsymbol{b}_{R2}$ is similar, the angles α_1 and α_2 between the vectors of matrix A and the corresponding

vectors of matrix $\boldsymbol{B_R}$ are similar (see Fig. 2), i.e. $\alpha_1 \approx \alpha_2 \approx \alpha$.

Using Eq (B17) (QR decomposition), matrix $\boldsymbol{T}$ is expressed as:

$$\boldsymbol{T} = \boldsymbol{R}_2\boldsymbol{Q}_{2a} \tag{C6}$$

i.e.:

$$[\boldsymbol{t}_1\, \boldsymbol{t}_2] = [\boldsymbol{r}_1\, \boldsymbol{r}_2]\begin{bmatrix} \boldsymbol{q}_{11} & \boldsymbol{q}_{12} \\ 0 & \boldsymbol{q}_{22} \end{bmatrix} \tag{C7}$$

From which it is inferred that the vector $\boldsymbol{t}_1$ coincide with vector $\boldsymbol{r}_1$ and, consequently, a slightly different rotation matrix is obtained (see Fig 2).

The mode shapes of system A can be expressed as:

$$[\boldsymbol{a}_1\, \boldsymbol{a}_2] = [\boldsymbol{b}_{R1}\, \boldsymbol{b}_R]\begin{bmatrix} \boldsymbol{q}_{11} & \boldsymbol{q}_{12} \\ 0 & \boldsymbol{q}_{22} \end{bmatrix} \tag{C8}$$

From which it is inferred that:

$$\boldsymbol{a}_1 = \boldsymbol{b}_{R1}\boldsymbol{q}_{11} \;\; ; \;\; \boldsymbol{a}_2 = \boldsymbol{b}_{R1}\boldsymbol{q}_{12} + \boldsymbol{b}_{R2}\boldsymbol{q}_{22} \tag{C9}$$

i.e. $\boldsymbol{a}_1$ coincide with $\boldsymbol{b}_{R1}$ whereas the angle between the other set of mode shapes is approximately 2α (or $\alpha_1 + \alpha_2$ if the angles are different).

APPENDIX D. EFFECT OF MODE SHAPE NORMALIZATION

In the equations derived in section 2, it was assumed that the mode shapes are mass-normalized.

If we denote the modal matrix with unscaled (not mass-normalized) mode shapes by $\boldsymbol{A_U}$, the modal matrices $\boldsymbol{A}$ and $\boldsymbol{A_U}$ are related by:

$$\boldsymbol{A} = \boldsymbol{A_U}\boldsymbol{\alpha_A} \tag{D1}$$

Where $\boldsymbol{\alpha_A}$ is a diagonal matrix containing the scaling factors.

The corresponding transformation matrices:

$$\boldsymbol{T} = \boldsymbol{B}^{-1}\boldsymbol{A} \tag{D2}$$

And

$$\boldsymbol{T_U} = \boldsymbol{B}^{-1}\boldsymbol{A_U} \tag{D3}$$

are related by:

$$\boldsymbol{T} = \boldsymbol{T_U}\,\boldsymbol{\alpha_A} \tag{D4}$$

The matrix $\boldsymbol{T}$ is factorized with the QR factorization as:

$$\boldsymbol{T} = \boldsymbol{R}_2\boldsymbol{Q}_{2a} \tag{D5}$$

Matrices $\boldsymbol{T_U}$ and $\boldsymbol{\alpha_A}$ can also be factorized using the QR decomposition as:

$$\boldsymbol{T_U} = \boldsymbol{R_{TU}}\boldsymbol{Q_{TU}} \tag{D6}$$

and:

$$\boldsymbol{\alpha_A} = \boldsymbol{R}_{\alpha_A}\boldsymbol{Q}_{\alpha_A} \tag{D7}$$

where $\boldsymbol{R}_{\alpha_A} = \boldsymbol{I}$ and $\boldsymbol{Q}_{\alpha_A} = \boldsymbol{\alpha_A}$. From Eqs. (D5-D7), it is derived that the matrices $\boldsymbol{R}_2$ and $\boldsymbol{Q}_{2a}$ can be expressed as:

$$\boldsymbol{R}_2 = \boldsymbol{R_{TU}} \tag{D8}$$

and

$$\boldsymbol{Q}_{2a} = \boldsymbol{Q_{TU}}\boldsymbol{Q}_{\alpha_A} = \boldsymbol{Q_{TU}}\boldsymbol{\alpha_A} \tag{D9}$$

which demonstrates that the QR decomposition of matrices $\boldsymbol{T}$ and $\boldsymbol{T_U}$ provides the same rotation matrix. However, this is not the case for the polar decomposition.

References

[1] J.E. Mottershead, M.I. Friswell, Model updating in structural dynamics: A survey, J. Sound Vib. 167 (1993) 347–375, https://doi.org/10.1006/jsvi.1993.1340.

[2] D.J. Ewins, Model validation: Correlation for updating, Sadhana. 25 (2000) 221–234, https://doi.org/10.1007/BF02703541.
[3] A. Rytter, P.H.P. Kirkegaard, Vibration based inspection of civil engineering structures, Aalborg University, 1994.
[4] G.. Stewart, J. Sun, Matrix Perturbation Theory, 1st ed., Boston, 1990. https://doi.org/10.1201/9781420010572-15.
[5] The University of Manchester, Helping Engineers Learn Mathematics, (n.d.).
[6] A. Sestieri, Structural dynamic modification, Sadhana. 25 (2000) 247–259, https://doi.org/10.1007/BF02703543.
[7] A. Sestieri, W. D'Ambrogio, A modification method for vibration control of structures, Mech. Syst. Signal Process. 3 (1989) 229–253, https://doi.org/10.1016/0888-3270(89)90051-4.
[8] M. Nad, Structural dynamic modification of vibrating systems, Appl. Comput. Mech. 1 (2007) 203–214.
[9] J.E. Mottershead, C. Mares, M.I. Friswell, An inverse method for the assignment of vibration nodes, Mech. Syst. Signal Process. 15 (2001) 87–100, https://doi.org/10.1006/mssp.2000.1353.
[10] A. Kyprianou, J.E. Mottershead, H. Ouyang, Assignment of natural frequencies by an added mass and one or more springs, Mech. Syst. Signal Process. 18 (2004) 263–289, https://doi.org/10.1016/S0888-3270(02)00220-0.
[11] Y.-H. Park, Y.-S. Park, Structural modification based on measured frequency response functions: An exact eigenproperties reallocation, J. Sound Vib. 237 (2000) 411–426, https://doi.org/10.1006/jsvi.2000.3041.
[12] B.P. Wang, L. Kitis, W.D. Pilkey, A. Palazzolo, Structural modification to achieve antiresonance in helicopters, J. Aircr. 19 (1982) 499–504, https://doi.org/10.2514/3.44769.
[13] W. D'Ambrogio, Some remarks about structural modifications involving additional degrees of freedom, Mech. Syst. Signal Process. 4 (1990) 95–99, https://doi.org/10.1016/0888-3270(90)90043-K.
[14] R.J. Pomazal, V.W. Snyder, Local Modifications of Damped Linear Systems, AIAA J. 9 (1971) 2216–2221, https://doi.org/10.2514/3.50028.
[15] J.T. Weissenburger, Effect of Local Modifications on the Vibration Characteristics of Linear Systems, J. Appl. Mech. 35 (1968) 327–332, https://doi.org/10.1115/1.3601199.
[16] H. Özgüven, Structural modifications using frequency response functions, Mech. Syst. Signal Process. 4 (1990) 53–63.
[17] W. D'Ambrogio, A. Sestieri, Coupling theoretical data and translational FRFs to perform distributed structural modification, Mech. Syst. Signal Process. 15 (2001) 157–172, https://doi.org/10.1006/mssp.2000.1368.
[18] H. Hang, K. Shankar, J.C.S. Lai, Prediction of the effects on dynamic response due to distributed structural modification with additional degrees of freedom, Mech. Syst. Signal Process. 22 (2008) 1809–1825, https://doi.org/10.1016/j.ymssp.2008.02.006.
[19] H. Hang, K. Shankar, J.C.S. Lai, Effects of distributed structural dynamic modification with reduced degrees of freedom, Mech. Syst. Signal Process. 23 (2009) 2154–2177, https://doi.org/10.1016/j.ymssp.2009.03.014.
[20] H. Hang, K. Shankar, J.C.S. Lai, Effects of distributed structural dynamic modification with additional degrees of freedom on 3D structure, Mech. Syst. Signal Process. 24 (2010) 1349–1368, https://doi.org/10.1016/j.ymssp.2010.01.002.
[21] P. Avitable, Twenty years of structural dynamic modification: A review, Sound&Vibration. (2002) 14–25.
[22] R. Brincker, A. Skafte, M. López-Aenlle, A. Sestieri, W. D'Ambrogio, A. Canteli, A local correspondence principle for mode shapes in structural dynamics, Mech. Syst. Signal Process. 45 (2014) 91–104, https://doi.org/10.1016/j.ymssp.2013.10.025.
[23] M. Aenlle, R. Stufano, N. García-Fernández, F. Pelayo, R. Brincker, Cross-Length of Mode Shapes in Structural Dynamics: Concept and Applications, Shock Vib. 2023 (2023) 1–16, https://doi.org/10.1155/2023/2745671.
[24] D. Bernal, Modal Scaling from Known Mass Perturbations, J. Eng. Mech. 130 (2004) 1083–1088, https://doi.org/10.1061/(ASCE)0733-9399(2004)130:9(1083).
[25] R. Brincker, M. Lopez-Aenlle, Mode shape sensitivity of two closely spaced eigenvalues, J. Sound Vib. 334 (2015) 377–387, https://doi.org/10.1016/j.jsv.2014.08.015.
[26] Q. Yang, X. Peng, An exact method for calculating the eigenvector sensitivities, Appl. Sci. 10 (2020), https://doi.org/10.3390/app10072577.
[27] R.B. Nelson, Simplified calculation of eigenvector derivatives, AIAA J. 14 (1976) 1201–1205, https://doi.org/10.2514/3.7211.
[28] T. Lyche, Numerical Linear Algebra and Matrix Factorizations, Springer International Publishing, Cham (2020), https://doi.org/10.1007/978-3-030-36468-7.
[29] G. Golub, C. Van Loan, Matrix Computations, 4th ed., Johns Hopkins University Press, 2013 https://doi.org/10.56021/9781421407944.
[30] W. Gander, Algorithms for the Polar Decomposition, SIAM J. Sci. Stat. Comput. 11 (1990) 1102–1115, https://doi.org/10.1137/0911062.
[31] N.J. Higham, Computing the Polar Decomposition—with Applications, SIAM J. Sci. Stat. Comput. 7 (1986) 1160–1174, https://doi.org/10.1137/0907079.
[32] N.J. Higham, R.S. Schreiber, Fast Polar Decomposition of an Arbitrary Matrix, SIAM J. Sci. Stat. Comput. 11 (1990) 648–655, https://doi.org/10.1137/0911038.
[33] C.R. Goodall, Computation using the QR decomposition, in: Handb. Stat., 1993: pp. 467–508. https://doi.org/10.1016/S0169-7161(05)80137-3.
[34] W. Gander, Algorithms for the QR-Decomposition, Zürich, 1980.
[35] R.A. Horn, C.R. Johnson, Matrix Analysis, Cambridge University Press (1985), https://doi.org/10.1017/CBO9780511810817.
[36] C. Lein, M. Beitelschmidt, Comparative study of model correlation methods with application to model order reduction. Proc. 26th ISMA (international Conf. Noise Vib, Eng, 2014.
[37] R.J. Allemang, D. Brown, Correlation Coefficient for Modal Vector Analysis, in: Proc. 1st Int. Modal Anal. Conf., International Society for Optical Engineering and Society for Experimental Mechanics, Orlando, 1982: pp. 110–116.
[38] R. Clough, J. Penzien, Dynamics of structures, McGraw-Hill, New York, 1993.
[39] R. Brincker, C.E. Ventura, Introduction to Operational Modal Analysis, John Wiley & Sons Ltd, Chichester, UK (2015), https://doi.org/10.1002/9781118535141.
[40] W. Heylen, S. Lammens, P. Sas, Modal analysis theory and testing, Katholieke Universiteit Leuven, Belgium, 2007.
[41] B.C. Hall, Lie Groups, Lie Algebras, and Representations, Springer International Publishing, Cham (2015), https://doi.org/10.1007/978-3-319-13467-3.
[42] J. Panetta, Polar Decomposition and the Closest Rotation (2015) 1–4.
[43] N.J. Higham, Applied mathematics, numerical linear algebra and software., What Is Polar Decomposition? (2020). https://nhigham.com/2020/07/28/what-is-the-polar-decomposition/.
[44] C. Jonscher, L. Liesecke, N. Penner, B. Hofmeister, T. Grießmann, R. Rolfes, Influence of system changes on closely spaced modes of a large-scale concrete tower for the application to structural health monitoring, J. Civ. Struct. Heal. Monit. (2023), https://doi.org/10.1007/s13349-023-00693-6.
[45] MATLAB Version 9.9.0 (R2020b) (2022).